AGU PUBLICATIONS

JGR

Journal of Geophysical Research: Planets

RESEARCH ARTICLE
10.1002/2013JE004583

Special Section:
Results from the first 360 Sols of the Mars Science Laboratory Mission: Bradbury Landing through Yellowknife Bay

Key Points:
- Distal end of Peace Vallis fan was near MSL landing
- Sediment in the fan was derived from valley incision into colluvium
- Fan morphology consistent with fluvial processes

Correspondence to:
M. C. Palucis,
mpalucis@berkeley.edu

Citation:
Palucis, M. C., W. E. Dietrich, A. G. Hayes, R. M. E. Williams, S. Gupta, N. Mangold, H. Newsom, C. Hardgrove, F. Calef III, and D. Y. Sumner (2014), The origin and evolution of the Peace Vallis fan system that drains to the *Curiosity* landing area, Gale Crater, Mars, *J. Geophys. Res. Planets*, *119*, 705–728, doi:10.1002/2013JE004583.

Received 22 NOV 2013
Accepted 25 FEB 2014
Accepted article online 3 MAR 2014
Published online 4 APR 2014

The origin and evolution of the Peace Vallis fan system that drains to the *Curiosity* landing area, Gale Crater, Mars

Marisa C. Palucis[1], William E. Dietrich[1], Alexander G. Hayes[2], Rebecca M. E. Williams[3], Sanjeev Gupta[4], Nicholas Mangold[5], Horton Newsom[6], Craig Hardgrove[7], Fred Calef III[8], and Dawn Y. Sumner[9]

[1]Department of Earth and Planetary Science, University of California, Berkeley, California, USA, [2]Department of Astronomy, Cornell University, Ithaca, New York, USA, [3]Planetary Science Institute, Tuscan, Arizona, USA, [4]Department of Earth Science and Engineering, Imperial College London, London, UK, [5]Laboratoire Planetologie et Geodynamique de Nantes, CNRS UMR 6112, Université de Nantes, Nantes, France, [6]Institute of Meteoritics, University of New Mexico, Albuquerque, New Mexico, USA, [7]School of Earth and Space Exploration, Arizona State University, Tempe, Arizona, USA, [8]NASA Jet Propulsion Laboratory, California Institute of Technology, Pasadena, California, USA, [9]Geology Department, University of California, Davis, California, USA

Abstract The landing site for the *Curiosity* rover is located at the distal end of the Peace Vallis fan in Gale Crater. Peace Vallis fan covers 80 km^2 and is fed by a 730 km^2 catchment, which drains an upland plains area through a 15 km wide gap in the crater rim. Valley incision into accumulated debris delivered sediment through a relatively low density valley network to a main stem channel to the fan. An estimated total fan volume of 0.9 km^3 matches the calculated volume of removal due to valley incision (0.8 km^3) and indicates a mean thickness of 9 m. The fan profile is weakly concave up with a mean slope of 1.5% for the lower portion. Numerous inverted channels outcrop on the western surface of the fan, but on the eastern portion such channels are rare suggesting a change in process from distributary channel domination on the west to sheet flow on the eastern portion of the fan. Runoff (discharge/watershed area) to produce the fan is estimated to be more than 600 m, perhaps as much as 6000 m, indicating a hydrologic cycle that likely lasted at least thousands of years. Atmospheric precipitation (possibly snow) not seepage produced the runoff. Based on topographic data, Peace Vallis fan likely onlapped Bradbury Rise and spilled into a topographic low to the east of the rise. This argues that the light-toned fractured terrain within this topographic low corresponds to the distal deposits of Peace Vallis fan, and in such a setting, lacustrine deposits are expected.

1. Introduction

On 6 August 2012, UTC, the Mars Science Laboratory (MSL) rover, *Curiosity*, landed in Gale Crater (5.3°S 137.7°E, Figures 1 and 2) within a landing ellipse (Figure 3) that partially included a hypothesized alluvial fan deposit [e.g., *Anderson and Bell*, 2010], now named the Peace Vallis fan. The actual landing site (Bradbury Landing) was a few hundred meters east of the distal end of this fan. The MSL team observed that the distal end entered an enclosed topographic low area and predicted that fine-grained sediment, including possibly lake deposits, would be found there. This contributed to the decision to first send *Curiosity* to the east rather than head directly to the base of Aeolis Mons [*Grotzinger et al*., 2014]. En route, water-transported gravels, outcropping as conglomerates [*Williams et al*., 2013a] were found and clay-bearing mudstones were discovered in Yellowknife Bay [*Grotzinger et al*., 2014; *Vaniman et al*., 2014]. These in situ observations confirm the ability to identify fluvial/alluvial facies from orbital data using geomorphic observations and will provide insight for the 100 other large alluvial fan deposits (> 10 km long downslope) that have been identified on the southern highlands of Mars, most originating in alcoves near crater rims [*Moore and Howard*, 2005; *Kraal et al*., 2008; *Wilson et al*., 2012].

These findings by MSL and previous studies of the other alluvial fans provide strong context for analysis of the Peace Vallis fan. *Moore and Howard* [2005] showed that the slopes of these crater rim-derived fans averaged about 2% were weakly concave up and, combined with fan size and catchment relief, suggested deposition by gravel-bedded rivers. They proposed that the lack of fan-head trenching in these features indicates an abrupt end to climatic conditions favorable to fan generation. Runoff from snowmelt was proposed to be the driver for erosion and fan generation.

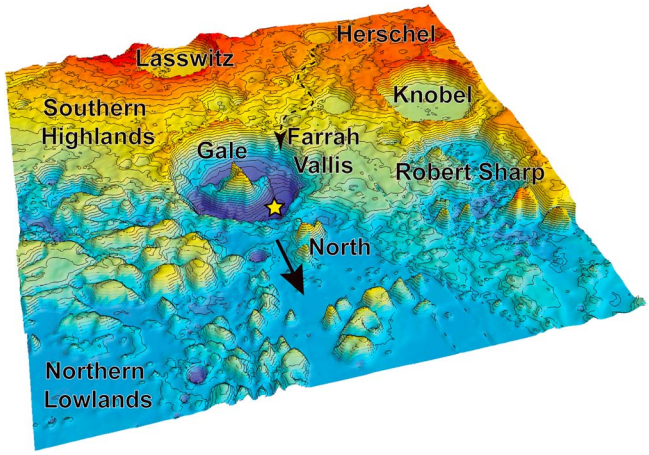

Figure 1. MOLA-derived topographic and elevation map of the Gale Crater region overlain with 250 m contours. Gale Crater is located on the crustal dichotomy between the cratered southern highlands and the smoother northern lowlands of Elysium Planitia, and it is this regional slope that contributes to the difference in elevation between the northern and southern rim. The lowest elevations in Gale Crater occur on the northwest portion of the crater floor, near the MSL landing site (denoted by a star). Recent crater counts on Gale's ejecta give an age estimate of ~3.6 ± 0.05 Ga, corresponding to the Early Hesperian or possibly the Late Noachian [e.g., *Le Deit et al*., 2013]. The black dashed line between Herschel crater and Gale Crater shows a possible paleoflow path for water into Gale Crater (based on *Irwin et al*. [2005]).

Irwin et al. [2005], building upon earlier work by *Cabrol et al*. [1999], hypothesized that in Gale Crater, specifically, there was a brief period in which highland valley networks were reactivated, drained toward Gale, and breached the crater rim, delivering water that caused lake and delta formation (Figure 3). Simultaneously, Aeolis Mons was gullied, the crater wall was cut by gullies, and fans formed. This would have occurred, therefore, after the Aeolis Mons sediments were deposited and then partially removed by wind erosion [*Malin and Edgett*, 2000]. *Irwin et al*. [2005] suggested the brief hydrologic activity occurred in the Late Noachian to Early Hesperian.

In the region to the south of Gale Crater, similarly sized craters appear substantially more degraded, are partially to nearly buried, and have subtle rim topography, indicating that they likely predate Gale Crater. Farah Vallis (the large canyon entering Gale from the south, Figure 3) may have been part of an extensive regional drainage system (270,000 km^2) originating near Hershel Crater (Figure 1). Ejecta from Gale Crater may have partly buried this valley network, implying that the network is superimposed by Gale Crater and was active before crater formation [*Irwin et al*., 2005]. It is this network that *Irwin et al*. [2005] hypothesize was reactivated, and subsequently delivered water to Gale Crater. More recently, H.E. Newsom et al. (Gale Crater and impact processes—Observations during *Curiosity*'s first 360 sols on Mars, submitted to *Icarus*, 2014) have mapped the valleys superimposed by ejecta and found that the ejecta are generally poorly incised, and many of the local slopes of the older valleys were altered by the Gale-forming impact, leading them to conclude that the valleys leading to fan and deltas within Gale Crater are fresh and unrelated to past activity.

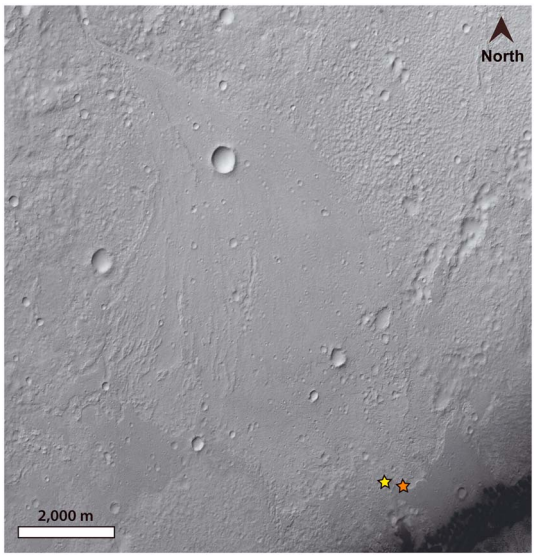

Figure 2. CTX imagery (6 m/pixel, image: P22_009571_1756_XI_04S222W) of the Peace Vallis fan. The location of the MSL *Curiosity* rover landing site (Bradbury Landing) is indicated by the yellow star, and Yellowknife Bay is indicated by the orange star. The fan apex is located in the northwest corner of the image and the fan spreads south and southeast.

Anderson and Bell [2010] produced the first detailed geomorphic map of Gale Crater (Figure 3), exploiting data from both the Mars Reconnaissance Orbiter (MRO) Context Camera (CTX) and the High-Resolution Imaging Science Experiment (HiRISE). They mapped features they labeled as "valley/canyons" on the crater rim and found that they are commonly branched, and many of them

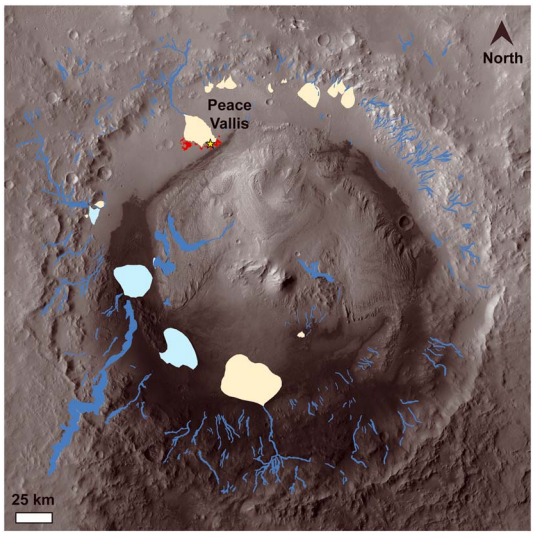

Figure 3. A modified version of the geomorphic map from *Anderson and Bell* [2010] showing their map of "valleys and canyons" (dark blue), "sinuous ridges" (white), and the Peace Vallis fan (labeled) which has cratered surfaces (red) surrounding its distal end. The cratered surfaces are part of *Anderson and Bell*'s [2010] "mound-skirting unit." Several large fans (tan) and fan deltas (light blue), including a large delta feature in the southwestern corner of Gale [*Irwin et al*., 2005], were added to their map.

along the northern rim lead to "fan-shaped mesas on the crater floor." Several of their mapped canyons also cut into Aeolis Mons in the center of Gale Crater. They propose that the valley/canyons and associated mesas are fluvial features, and they interpret the sinuous ridges found on the valley floor to be inverted channels (also referred to as exhumed channels [e.g., *Clarke and Stoker*, 2011]). In some cases, canyons lead downslope to sinuous ridges, and at several locations the sinuous ridges show a sinuosity characteristic of meandering rivers (e.g., a sinuosity of 2.0). Throughout the crater wall and floor, *Anderson and Bell* [2010] map a unit they label as the "mound-skirting unit" which they describe as a mesa-forming material that is intensely pitted and/or has parallel ridges. The mesas bordering the Peace Vallis fan are shown in Figure 3.

Anderson and Bell [2010] divided the 80 km^2 Peace Vallis fan into an upper, smooth lower thermal inertia unit and a lower, rocky light-toned and fractured, high thermal inertia unit. On the upper fan they noted ridges that they interpreted to be inverted channels or remnants of debris flows. They proposed that the high thermal inertia portion of the fan has been exposed by erosion of the overlying low thermal inertial unit.

Here we exploit HiRISE and CTX imagery, including photogrammetrically derived digital elevation data, to explore three questions: (1) What is the source of sediment comprising the Peace Vallis fan, (2) What processes formed the fan, and (3) How did the fan evolve though time? A detailed topographic analysis of Peace Vallis fan and its source area is presented. The eroded volume resulting from valley incision in the source area is then compared with the estimated volume of the fan. These analyses and observations are then collected to explore the three posed questions.

2. Methodology

2.1. Topographic Data

As part of the entry, descent, and landing (EDL) modeling effort for the MSL mission, comprehensive visual and topographic data sets were assembled for the landing ellipse and Peace Vallis fan in Gale Crater [*Golombek et al*., 2012]. Twelve MRO HiRISE 0.25 cm/pixel stereo pairs (created by the U.S. Geological Survey (USGS) Astrogeology Center in Flagstaff, AZ), three 6 m/pixel stereo pairs from the MRO CTX, and a crater-wide 50 m/pixel digital elevation model (DEM) made from Mars Express Orbiter High-Resolution Stereo Camera (HRSC) images were georeferenced and mosaiced to form the base of a geographic information system data set. These combined data sets form a "resolution pyramid" to allow mapping within Gale Crater at scales all the way down to a few meters or less. Data sets were projected into an equidistant cylindrical projection with zero as the center longitude and latitude, on a spherical Mars with a radius of 3,396,190 m. The resulting grid was used to extract 0.25 cm/pixel HiRISE visible, 1 m/pixel elevation, and 100 m/pixel thermal inertia data [*Parker et al*., 2013], and these data were provided to the MSL team. Most of the analyses presented here were derived from this topographic data set (see Table 1). These data were also georeferenced relative to a spheroid, as opposed to a geoid, to get delta radii elevations, which were used mainly by the entry, descent, and landing (EDL) team for EDL simulations [*Golombek et al*., 2012]. We used this data set when working with the lower fan and in the vicinity of the landing site/Yellowknife Bay, as it had fewer topographic artifacts than the MSL DEM.

Table 1. Data Sources Used for Each Analysis

Analysis	Data Source
1. Fan planform (contours, extent, long profiles)	HCN DEM
2. Sediment budget	MSL DEM, CTX
3. Paleochannels	MSL DEM
4. Catchment characteristics	MSL DEM, CTX
5. Fan reconstruction/mini-fan	Delta Radii DEM
6. Lake levels/gale fans and deltas	HRSC DEM, CTX
7. Crater counts	MSL DEM, CTX DEM, CTX

In addition to the DEMs provided to the MSL team by the USGS at Flagstaff, we also created a 1 m resolution topographic data set using a controlled network of nine HiRISE stereo images, herein referred to as the HCN (HiRISE Controlled Network) DEM. The images were controlled using 280 Mars Orbiter Laser Altimeter (MOLA) shots and 240 tie points spread throughout the HCN DEM boundary (Figure 4). The tie points were given *z* control (elevation) using a four-image CTX DEM. This HCN DEM was developed to improve upon the MSL-provided DEM, which had several major artifacts along image boundaries down the center of the Peace Vallis fan, preventing an accurate analysis of the fan's planform topography. As shown in Figure 4, MOLA points along the edges of the HiRISE DEMs are generally sparse, making it difficult to mosaic the various HiRISE DEMs together without topographic artifacts. Several points on the fan were chosen to compare the MOLA elevation values with those extracted from the MSL DEM and our HCN DEM. The MSL model varied by 2–5 m compared to the MOLA data, while our HCN DEM was typically within a meter of the MOLA values. In comparing relative elevation differences though, such as when determining the deflation depth of ridges on the fan, both the MSL and our HCN model provided similar results.

For areas outside of the landing ellipse and alluvial fan, CTX and HRSC data were primarily used. A radiometrically calibrated CTX mosaic at 6 m/pixel was provided by the MSL team and was used mainly to identify topographic features. For crater-wide context at Gale, a HRSC-derived topographic map, also provided by the MSL team, at a resolution of 50 m/pixel, was used.

2.2. Volume Calculations

Much of the topographic analysis presented here relies on methods similar to those developed by *Warner et al.* [2011] for basin volumes and *Chaytor et al.* [2009] for landslide volumes. The volume eroded from the lower main stem of the valley network in the source area was calculated by projecting a smooth surface between the bounding sidewalls on either flank of the valley, essentially creating a "lid" over the lower incised valley network. This projected surface was then gridded and subtracted from the original gridded topography. Our methodology used ArcGIS tools, though all postprocessing was conducted in MATLAB. To estimate the fan volume, we first eliminated the topographic data under the fan and projected the topography laterally from the east and west to create a pre-fan surface. We then took a difference between the gridded fan surface and this projected surface to estimate the volume of the fan.

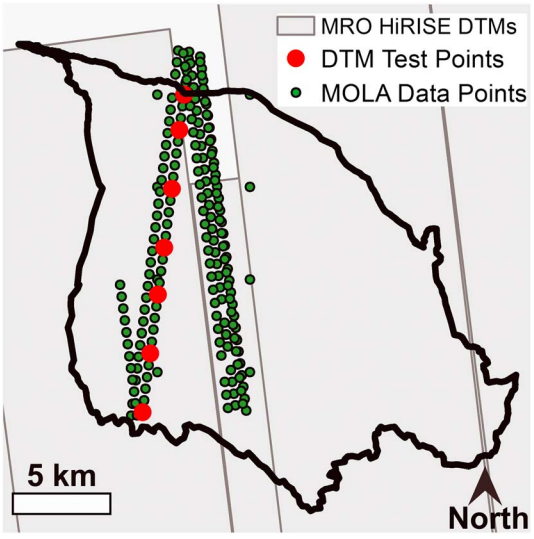

Figure 4. The location of MOLA data points (green) in the vicinity of the Peace Vallis fan. DEM test points (red) were used to compare MOLA elevations with those extracted from the MSL DEM and the HCN DEM created for this manuscript. The scarcity of MOLA data along the edges of the HiRISE stereo images (footprints shown in grey) prevents a data project that is wholly free from topographic artifacts.

We used three different interpolation methods for determining the pre-fan topography. The first uses a nearest-neighbor interpolation using only points within the first 500 m outside of the fan's edges, the second projects polylines connecting contours on the eastern edge of the fan to the same contours on the western edge, and the third uses the contours on either side of the fan as a guide to the topography beneath the fan. For the second and third interpolations, we

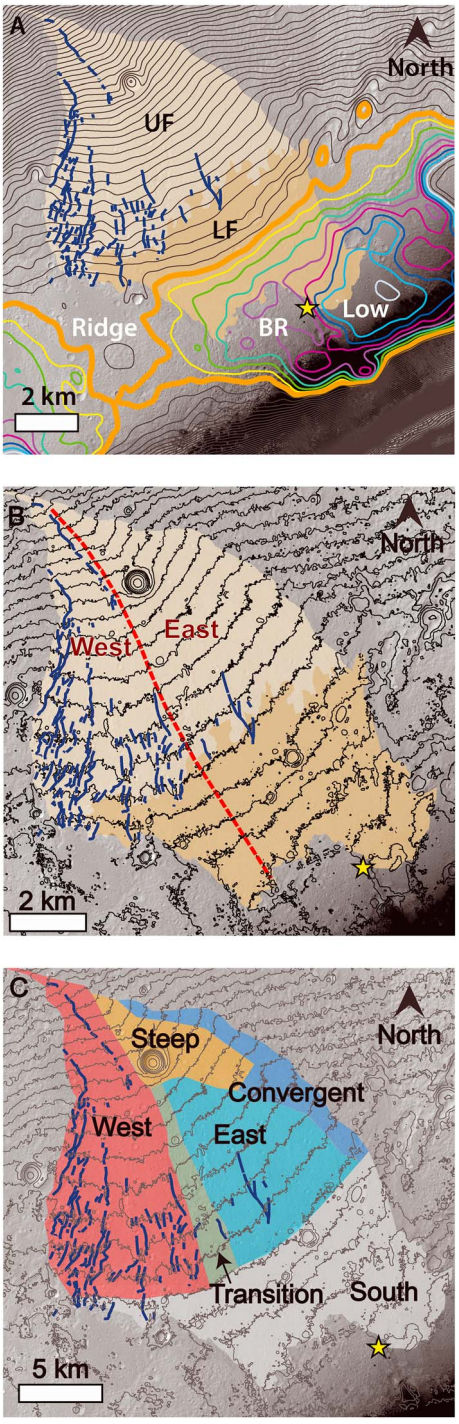

Figure 5

assign elevation values to points created from polylines and then use those points, in addition to the points around the fan's edges, to perform a nearest-neighbor interpolation. In the first case the pre-fan topography has an unrealistic bulge where the crater wall meets the floor, the second creates a more planar surface under the fan, and the third creates a concavity (in planform) in the crater wall.

In order to reconstruct the fan topography immediately after its deposition (pre-wind erosion), all of the point elevation data from areas that show extensive erosion were excluded. These excluded data mostly occurred in the distal fan area where extensive wind erosion is evident. Here just the local erosion resistant mesas and outcrops were included to guide construction of the original fan surface. For the fan surface reconstruction we solved Laplace's equation in three dimensions and evaluated the resulting topography in the areas where the point elevation data had been removed. Comparison of the 5 m contours generated from the modeled surface to the actual 5 m contours over the uneroded terrain showed good agreement. The gridded reconstructed surface was then subtracted from the original gridded topography to create an erosion map for the lower Peace Vallis fan. In order to reduce computation time, all computations were done at a slightly coarser resolution of 2 m, instead of the native 1 m.

Topographic data to determine erosion caused by valley incision in the source area are limited. There is only HiRISE DEM coverage for the lower main stem of Peace Vallis, and CTX DEM data are too coarse to resolve the smaller channels higher up in the drainage network. We therefore used the area for which we had high-resolution DEM data to determine width-to-depth relationships for the incised valleys. We then extended this relation to the entire channel network so that in areas where coverage was limited to visual data alone, measured channel widths could be used to estimate a channel depth. By doing this along the entire channel network (a length of over 107 km), volume of material missing from the headwaters was estimated. Since cessation of channel incision, dust and colluvium have partially infilled these channels. The limited coverage of HiRISE imagery of the source area suggests that there may have been some finer-scale branching network. Hence, our estimate of sediment produced by channel incision may be somewhat low.

3. The Peace Vallis Fan

3.1. Planform, Materials, and Topographic Boundary Conditions

Peace Vallis fan is a depositional feature on the northern inner wall of Gale Crater that is expressed by convex contours relative to the surrounding crater walls (Figures 3 and 5 and Table 2). *Anderson and Bell* [2010]

Table 2. General Properties Used to Describe the PEACE Vallis Fan System

Property	Value	Range	Units	Data Source
Catchment drainage area	730		km^2	CTX
Catchment relief	2		km	HRSC
Catchment valley length	107		km	CTX
Catchment valley width	300	80–900	m	HiRISE, CTX
Catchment valley eroded volume	0.77	0.7–0.9	km^3	HiRISE, CTX
Catchment valley average slope	0.05	0.025–0.07	--	CTX
Catchment drainage density	0.15	--	km	CTX
Fan surface area	80		km^2	HiRISE
Upper	49	--	km^2	
Lower	31		km^2	
Fan volume	0.9		km^3	HiRISE
Current	0.7	0.4–0.8	km^3	
Eroded	0.2	0.15–0.25	km^3	
Average fan depth	7		m	HiRISE
East	6	4–9	m	
West	8	4–11	m	
Overall fan gradient				HiRISE
East	1.2		--	
West	1.5		--	
Fan paleochannel width	27	7–110	m	HiRISE
Fan paleochannel deflation depth				HiRISE
East	0.6	0.3–1	m	
West	2.4	0.5–5	m	
Fan relief	275	--	m	HiRISE
Fan apex angle	60	--	degrees	HiRISE
Dist. apex to Bradbury Landing	15.2	--	km	HiRISE

mapped the outline of the fan using geomorphologic characteristics and thermal inertial data. We independently mapped the fan boundary based on the topographic boundary of the characteristic contours. Our map, which shows minimal differences to that of *Anderson and Bell* [2010], is used here. The fan is modest in size compared to other alluvial fans on Mars [*Moore and Howard*, 2005], covering approximately 80 km^2.

The fan's apex is located about ~10 km downslope from the crater rim and 900 m down in elevation, below which the fan spreads 60° down to a complex valley floor. Here the fan encountered three lower topographic boundary conditions (Ridge, Bradbury Rise, and Low, Figures 5 and 6). The western side of the fan extends to a flat-topped broad ridge that continues across to Aeolis Mons. This ridge defines the western border of a 64 km^2 enclosed topographic low area (up to 45 m deep) that extends 14.5 km to the east (Figure 6a). The enclosed low contains two highs: Bradbury Rise (the *Curiosity* landing area) and a second topographic rise to the east that is somewhat lower in elevation than Bradbury Rise. These are separated by a local low (15 to 25 m lower than Bradbury Rise) (Figures 5a and 6a), which includes the informally named Yellowknife Bay and a second, larger low area that lies at the eastern end of the enclosed area (Figure 6a). The distal end of the fan extends into the enclosed topographic low area, potentially onlapping Bradbury Rise, and descends into the adjacent local low (in the vicinity of Yellowknife Bay). Bradbury Rise is relatively flat, but it does have a mean southeastern slope toward Aeolis Mons. The relatively flat surface south of Yellowknife Bay also slopes weakly toward Aeolis Mons. The convexity of the fan contours flatten out (but remain convex) just as the central and eastern portions of the fan enter this enclosed topographic low (Figure 6b). All three of these lower topographic boundaries (i.e., Ridge, Bradbury Rise, and Low) are bordered by nearly flat-lying dark cratered surfaces (referred to as the "mound-skirting unit" by *Anderson and*

Figure 5. (a) *Anderson and Bell* [2010] divided the Peace Vallis fan into an upper smooth, lower thermal inertia unit and a lower "high, thermal inertia unit." Shown here is a revised mapping of their upper/lower fan boundary by the MSL team, where the upper fan (UF) is shown in tan and the lower fan (LF) is shown in light brown. Overlain on the mapping are 5 m smoothed HiRISE contours, which show the continuation of the fan form from the upper to lower fan. The western edge of the fan terminates on a flat-topped broad ridge, while the eastern fan enters into an enclosed basin (denoted by the thick orange contour) that contains Bradbury Rise and spills into a local topographic low. From HiRISE imagery, 43 distinct ridges were mapped (blue). (b) The 5 m smoothed contours have been replaced by 10 m contours created from the HCN DEM. A red dashed line denotes a division between the western fan, which slopes to the south and contains most of the mapped ridges, and the eastern fan, which has few ridges and spills to the southeast into the enclosed basin. (c) Contour map of 10 m with topographic domains highlighted that may record specific phases or process changes in fan development. The distinction is defined by areas that share a common planform curvature, as determined by estimating a focus of radiation and fitting lines of constant arc to successive contour lines.

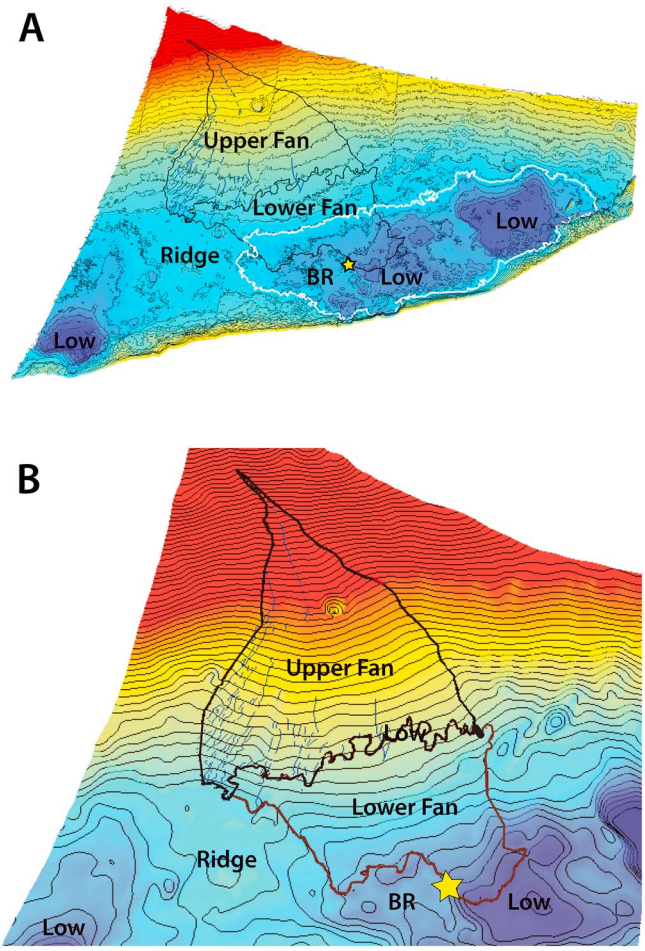

Figure 6. (a) A three-dimensional view of the Peace Vallis fan system (vertical exaggeration of 10) with a colorized elevation map and 10 m HiRISE contours. Adjacent to the "ridge" and within the enclosed basin (denoted by the thick white contour) is Bradbury Rise ("BR"), and to the east of Bradbury Rise is a local low into which the lower fan enters. A second, larger low lies adjacent to the eastern border of the enclosed basin. (b) The three boundary conditions discussed in section 3.1 (Ridge, Bradbury Rise, and Low) are highlighted.

Bell [2010] and as "cratered surface unit" by *Grotzinger et al.* [2014] and described above, as shown in Figures 3 and 7a).

Anderson and Bell [2010] divided the fan into an upper (northern) "smooth, lower thermal inertia unit" and lower (southern) "rockier, high thermal inertia unit." They extensively illustrate their descriptions with HiRISE and Thermal Emission Imaging System (THEMIS) images. The boundary between the upper and lower fan was remapped by the MSL team using these and other properties, including bedding and fractures, and are reported in *Grotzinger et al.* [2014] as "alluvial fan" and "light-toned, bedded fractured unit." Here we simply refer to the two distinctive areas that comprise the Peace Vallis fan as the upper fan (UF) and lower fan (LF) areas, with *Anderson and Bell*'s [2010] light-toned, bedded fractured unit comprising the distal portion of the alluvial fan. The upper fan outcrops over 49 km^2 and extends from the fan apex down to two thirds of the way to the distal margin (Figures 5a and 5b). It is characterized by a relatively smooth, mottled surface (Figure 8a) that corresponds to the low thermal inertia unit. Frequent, lighter toned, roughly circular patches of presumably infilled craters create the mottled appearance. Boulders, perhaps mostly produced by impacts, are scattered across the surface. Subtle blocky fractures, locally strongly expressed, can be found across the upper fan. With the exception of a few sharp-edged small craters which are bordered by ejecta of boulders and darker toned material, the craters have rounded edges and are partially to mostly infilled.

The lower fan, which covers 31 km^2, is characterized by lightly to heavily fractured, laterally extensive bedrock with scarps interpreted as bedded strata (Figure 8b). Extensive wind scour has etched the fractures and exposed the strata. In the transition zone between the upper and distal fan, the mottled and fractured surfaces are intermixed (Figure 8b) [*Sumner et al.*, 2013]. Farther downslope to the southeast, the lower fan becomes more deeply fractured, though the sizes of the polygonal fractures do not vary downslope systematically, either with distance or stratigraphy [*Hallet et al.*, 2013; *Sumner et al.*, 2013]. Boulders are rare and appear to be associated with the remnants of impact ejecta. Direct observation by MSL of the lower fan, high thermal inertia unit, in Yellowknife Bay indicates the presence of mudstones (Sheepbed member) and sandstones (Gillespie member) consistent with a distal fan location or lacustrine environment [*Grotzinger et al.*, 2014]. In contrast to the upper fan, the crater walls tend to be sharper edged, as controlled by underlying bedrock resistance. Wind-scoured elongated troughs across the exposed bedrock may originate as small craters (Figure 8c).

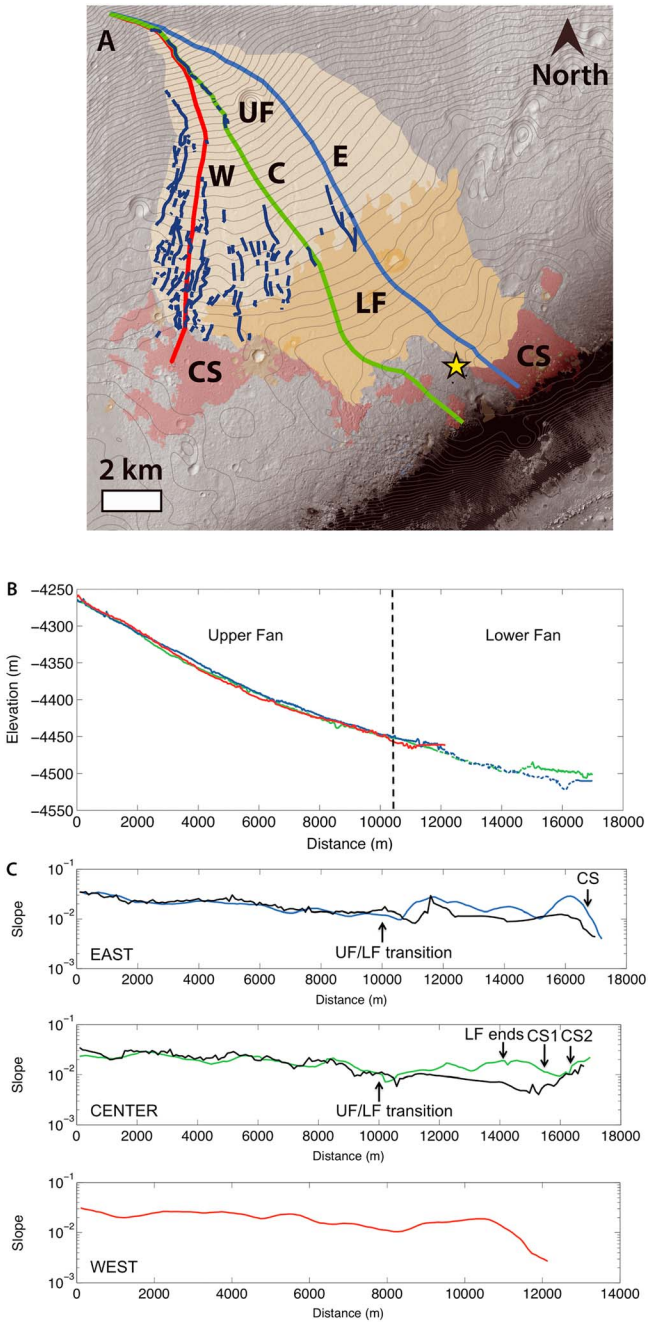

Figure 7

Topographically, the Peace Vallis fan differs from west to east (Figure 5b). The western portion of the fan (55 km^2) extends mostly from the apex toward the south and has numerous elongated, discontinuous ridges that are well expressed at the distal end. As discussed, these ridges appear to record exhumed paleochannels. The lower fan material (light-toned, fractured unit of *Anderson and Bell* [2010]) is absent near the far western margin. The eastern portion of the fan extends toward the southeast and has only a few subtle ridges that may record paleochannels. Finer-scale topographic domains in the upper fan may record specific phases or process changes in fan development, whereas the lower fan is composed of a single topographic domain (Figure 5c). The distinction among domains is defined by areas that share a common planform curvature, as determined by estimating a focus of radiation and fitting lines of constant arc to successive contour lines. The "west" domain is the most southward directed, contains most of the paleochannels, and has larger-scale ridge and swale topography across the lower end (Figure 5c). The "steep" domain is a local area of common curvature (distorted by a large impact crater) near the fan apex. Below it the "east" domain shows common curvature, has limited paleochannels, and ends in the light-toned, fractured bedded material composing the "south" domain. Bordering the fan, but still part of the fan based on mean contour orientation and surface texture, is a weakly topographically convergent area. This area appears to connect to a trough that runs along the lower eastern margin of the fan. A narrow transition area down the center of the fan does not correspond in form to either the west or east. In the south fan domain, contours share a common curvature for nearly the entire fan width. This domain corresponds to most of the light-toned, fractured bedded unit with high thermal inertia.

3.2. Profile Analysis

The fan slope decreases progressively from 3% at the apex to 1% at the upper-lower fan transition with significant lateral variability across the lower fan (Figure 7). Longitudinal profiles through the west, central, and east portions of the fan are similar from the apex down to the transition to the lower fan. Farther

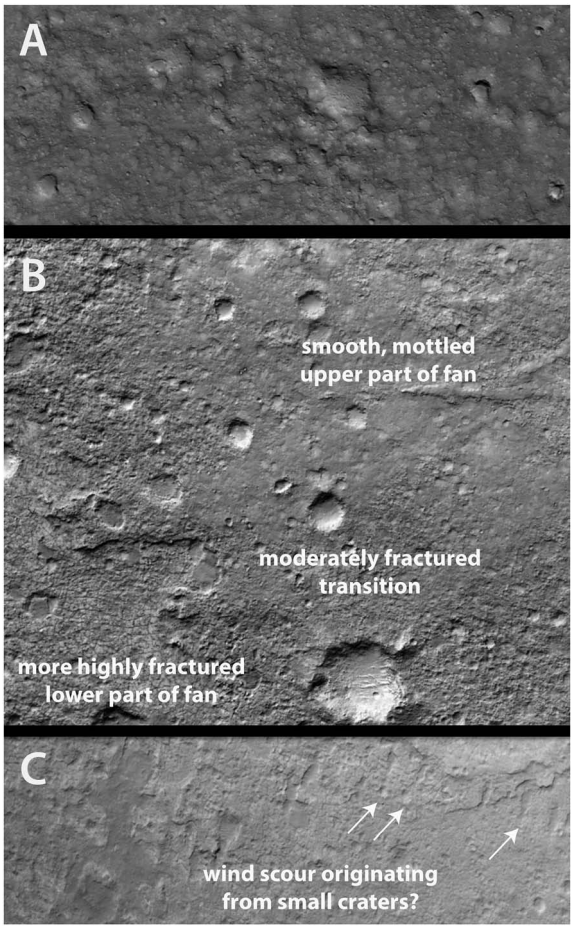

Figure 8. HiRISE imagery (0.25 m/pixel) of the Peace Vallis fan. (a) The upper fan is characterized by a relatively smooth, mottled surface that corresponds to the low thermal inertia unit (image: PSP_003453_1750_RED), (b) in the transition zone between the upper and distal fan, the mottled and fractured surfaces are intermixed (image: PSP_003453_1750_RED), and (c) wind-scoured elongated troughs across the exposed bedrock may originate as small craters (as indicated by the white arrows) (image: ESP_018920_1755).

downslope, the profiles differ greatly, depending on the pre-existing topography upon which the fan encroached. The lower portion of the shorter western profile is steeper than the others at equivalent distances downslope but then abruptly decreases as it crosses the cratered surface lying on the broad ridge at its base. The central and eastern profiles are nearly identical from the apex to the transition from the upper to lower fan, but the elevation and location of the topographic variations at the base of the fan clearly influence the profile shape (Figure 7b). The plot of the logarithm of slope versus distance shows a nearly linear relationship from the apex to the upper-lower fan transition, consistent with the profile being weakly exponential in form. Below this transition the current topography steepens into an enclosed topographic low with exposed bedding that is attributed to wind deflation. The topographic profile does not show abrupt changes when original topography is reconstructed (see section 2.2). The lower boundaries beyond the mapped extent of the fan have surface slopes toward Aeolis Mons (positive slope), and in the case of the profile across Bradbury Rise (the center profile), the slope progressively steepens from a low of about 0.4% (across the cratered surface) to greater than 1% (Figure 7). As discussed below, this suggests that although the distinct fan morphology does not extend across these surfaces, transport from the fan across these areas seems probable.

3.3. Paleochannels on Peace Vallis Fan

A system of downslope-oriented ridges in the western portion of the fan are visible in CTX imagery (Figure 2). The ridges are weakly sinuous, discontinuous, variable in width, and appear threaded together as compared to forming a branching network. The most continuous and uniform in width (35 ± 5 m) is a ridge about 3950 m

Figure 7. (a) The location of three longitudinal profiles down the fan are shown; each profile starts at the fan apex and terminates across one of the lower three boundaries discussed in section 3.1. The western profile (W, red) terminates on a cratered surface to the west (CS), the center profile (C, green) runs onto and across Bradbury Rise, and the eastern profile (E, blue) terminates on a cratered surface to the southeast. (b) Elevation versus distance data (extracted from the HCN DEM) are plotted for the three longitudinal profiles drawn in Figure 7a. The dashed line marks the boundary of the upper and lower fan. All three profiles are similar in form but begin to differ as they approach their lower boundary. For the center and eastern profiles the portion of the profile most heavily influenced by erosion is shown as dashed lines. Ignoring the lower boundaries, all three profiles have relatively low profile concavities of ~0.0002, similar to concavities measured by *Moore and Howard* [2005] for terrestrial and Martian fans of similar slope (1.5%). (c) The average fan slope was calculated every 100 m and the 10-point average was plotted as a function of distance for each of the three longitudinal profiles. For the eastern and center profiles, a constructed fan profile, which accounts for postdepositional fan erosion, is also plotted (black). In each case the longitudinal profiles progressively decline from 3% at the fan apex, down to 1%, at which point the fan slope is controlled by preexisting topography. The transition from the upper fan (UF) to the lower fan (LW) is marked for the center and east profiles.

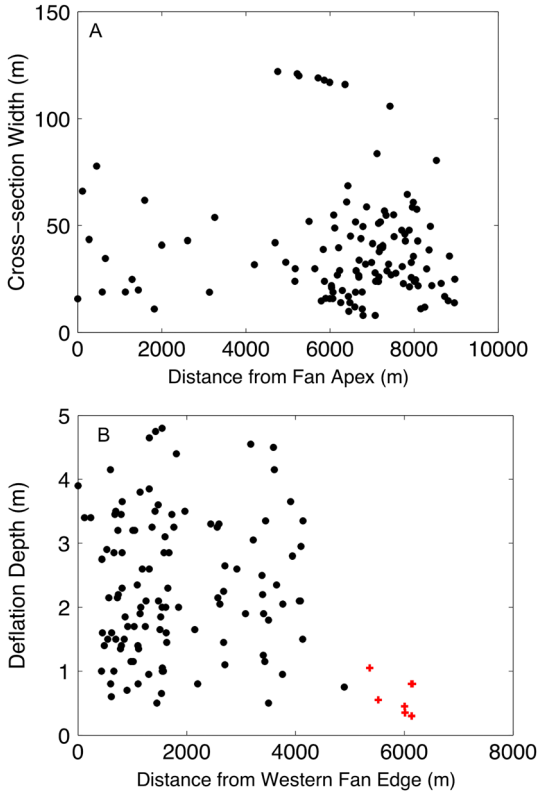

Figure 9. Cross-sectional data were extracted at 122 locations across the mapped ridges, interpreted to be paleochannels, using MSL DEM data to determine the average ridge width and deflation depth. (a) Cross-sectional width versus distance from the fan apex shows that there is no systematic change in ridge width as a function of distance downslope. (b) Deflation depth going from the edge of the western fan to the eastern fan shows a marked difference between the western and eastern fan, with an average depth of 2.4 m and 0.6 m, respectively.

long that originates near the fan apex and descends past the largest impact crater on the fan. We interpret these ridges as recording the coarser beds of various channels, preserved from wind deflation relative to finer-grained adjacent sediments (Figures 5–7). Collectively, the ridge topography in the lower western fan suggests either a braided channel system or intersecting stacked channels cut to a similar depth. Either geometry differs markedly from the sinuous, uniform width features that radiate across other Martian fans [e.g., *Morgan et al.*, 2014]. In the eastern fan, there are few, relatively narrow and uniform width ridges, one of which branches as it crosses from the upper to low fan units (Figure 5). Elsewhere (Figure 3) on Gale's wall and floor, and on the south side of Aeolis Mons, well-defined, uniform width, branching, sinuous ridges likely record single-thread channels (as mapped by *Anderson and Bell* [2010]).

Detailed cross-sectional and longitudinal profile analysis was done (using 1 m HiRISE digital elevation data) across these ridges to estimate paleochannel width and slope and deflation depth (local ridge height relative to adjacent plain). For 122 cross sections, we classified cross-section types following *Williams et al.* [2013b, Figure 4]. The ridges range in shape from flat topped to rounded to pinnacle, with either single, double, or triple peaks. Most of the ridges are predominately rounded to pinnacle shaped, as opposed to flat-topped, in profile. If the multiple peaks preserve multiple channel threads (consistent with braided channel network where the braid bars have eroded relative to the channel floors), the average channel width and standard deviation is 27 m ± 16 m, but if the multiple peaks represent a single channel, the average width and standard deviation is 34 m ± 18 m. The distribution of widths is approximately Gaussian, and width does not vary systematically with slope or distance downstream (Figure 9a).

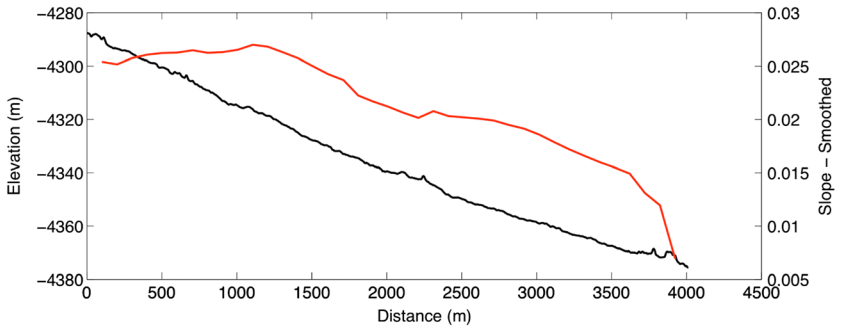

Figure 10. A longitudinal profile (black line) for the uppermost paleochannel on the Peace Vallis fan. Elevation data were extracted from the HCN DEM and plotted as a function of distance on the left *y* axis. Slope was calculated every 100 m, and the 10-point average is plotted as a function of distance. The slope declines from 2.5% near the fan apex to 1.5% near where the channel terminates.

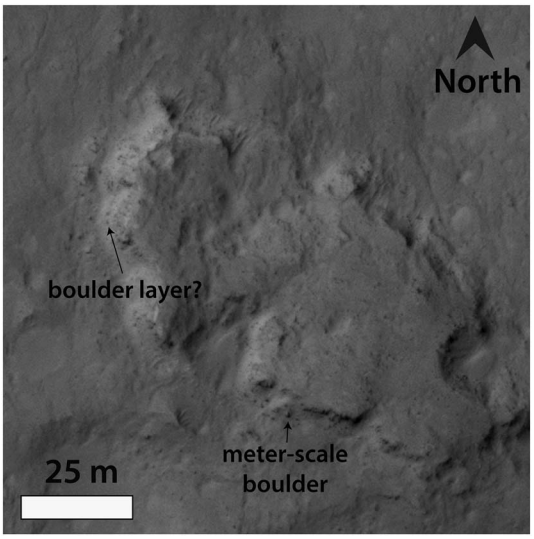

Figure 11. HiRISE image PSP_009716_1755 (25 cm/pixel resolution) showing a close-up of the main central ridge located near the fan apex. The ridge is ~50 m wide and shows alternating layers of light-toned material and darker boulder-rich deposits that are approximately 0.25 to 1 m thick. The individual boulders exposed in the outcrops in some of these channel deposits are meter to submeter scale; and they appear to decrease in density with distance from the ridge.

Deflation depth, determined from ridge height, averaged 2.4 m on the western fan and only 0.6 m on the eastern fan (Figure 9b), which is approaching the vertical resolution of the MSL DEM elevation data. The height of the ridges above the surrounding fan surface does not necessarily reflect the depth of the paleochannel but rather the deflation of the less protected fan surface. The inverted channel ridges are presumably resistant to erosion due to a lag of coarser rocks or cementing of channel deposits [*Newsom et al*., 2010]. The ridge profiles parallel the local fan slope. For the channels on the western fan, the average slope and standard deviation obtained from our long profile analysis is 1.9 ± 0.6%. The channel longitudinal profile for the 3950 m long paleochannel declines in slope from 2.5% near the apex to 1.5% near where the channel terminates (Figure 10). Hence, the downslope decrease in slope that typifies this fan occurs within a single channel.

Exposures on the sides of the ridges marking the paleochannels reveal some characteristics of the underlying deposits on the upper fan. Stratified layers of light-toned material and darker boulder-rich deposits are visible within many of the ridges on the upper and distal western portion of the fan (Figure 11). The alternating layers are on the order of 0.25 to 1 m wide in plan view, and there are typically three to five visible layers in most ridges. The individual boulders are meter to submeter scale, and their size distribution within and near the inverted channels appear to be fairly uniform, in contrast to variable-size distributions of boulders observed in the vicinity of impact craters elsewhere on the fan. There is an apparent decrease in the number of boulders with distance away from the inverted channels, which is a pattern that has been observed elsewhere on Mars [see *Williams et al*., 2011, Figure 3]. On the western rim of the largest impact crater on the upper fan surface is a dark band that may be an exposed boulder-rich layer. Boulders are found less frequently in the lower inverted channels on the western portion of the fan, and we have not observed boulders associated with the channels on the eastern fan. Boulders may have been transported down the fan as coarse-grained sediment or may have originated as weathering products of more indurated interbeds.

4. Peace Vallis Source Area

The northern Gale Crater rim is well defined by elevated topography relative to the Gale walls and floor to the south and to the adjacent plains beyond the crater to the north. Peace Vallis fan lies downslope from the largest extent of crater rim that is setback or breached (about 6 km) relative to the general position of the rim along the north (Figure 12a). This roughly 15 km long setback causes a topographic break in the rim that provides a drainage pathway from the northern plains; this extends more than 10 km to the north of the Gale Crater rim (Figure 12a). Using the current surface topography to infer the direction of transport of water and sediment, we can delineate the equivalent of a watershed area (or catchment) of about 1000 km^2 that may drain to the Peace Vallis fan (Figure 12a). This potential source area consists of steep hills along the offset rim, and then further north, gently sloping plains bordered and interspersed with local hills roughly 100 to 350 m in relief. The hills are not systematically cut by a network of canyons, suggesting no fluvial organization of this topography since impact and are perhaps the result of an irregular distribution of impact ejecta. In contrast, the broad plains to the west and east of the back-set rim show a mean slope toward the two entrance points to the steep canyon rising up from the fan apex (Figure 12a). CTX images of this area (no HiRISE coverage is available) reveal limited bedrock outcrops only at local steep portions of hilltops. Instead, these irregular hills

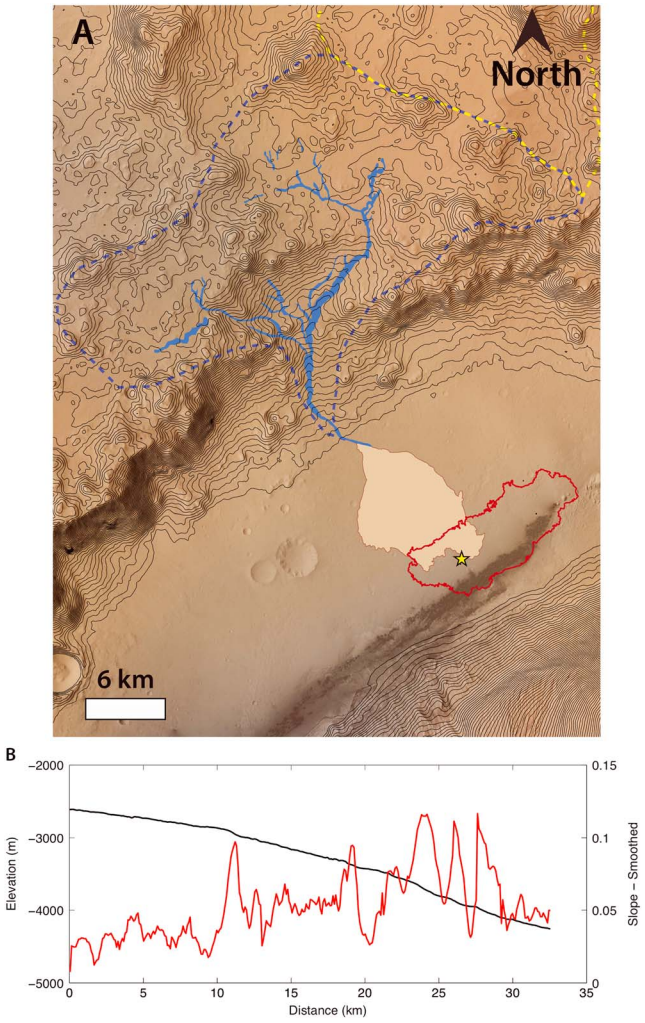

Figure 12. (a) Peace Vallis fan emanates from a well-defined incised valley network (light blue) located within a large topographic drainage area. The lower catchment (730 km^2) is dashed in blue, and the upper catchment (291 km^2) is dashed in yellow, such that an area of 1021 km^2 can drain to the outlet valley. HRSC contours of 50 m are shown for the catchment region only (starting above the fan apex) to highlight drainage from the upper plains, where the most distal tips of the valley network originates and the canyon from which the incised valley network emanates. The large enclosed basin into which the lower eastern portion of the Peace Vallis fan spills is outlined in red. "A" marks the start of the longitudinal profile shown in Figure 11b and "B" marks the end. (b) Elevation data were extracted and plotted as a function of distance (from a CTX-derived DEM) on the left *y* axis (black line) and on the right *y* axis; the slope was calculated every 100 m, and the 10-point average is plotted as a function of distance (red line). The average valley slope in the upland plains is roughly 0.02 (from 0 to 10 km), while the main stem reaches slopes locally of 0.1, which is in the mass flow regime for sediment transport.

are mostly mantled with debris, which appear to be some combination of eolian deposits and colluvium. The gross slope of the plains surface toward the outlet, the apparent ramps of colluvium off adjacent hills to the plains, the basin-like topography in which the plains are located, and the occurrence of local ridges (both within the source area and adjacent regions) that may record depositional features elevated due to deflation, all suggest that the plains are underlain by mixtures of colluvium, fluvial, and eolian sediments. These areas may also collect ash fall, as a large area of volcanic plains lies to the north.

Cut into the debris mantle in the source area is a spatially limited, relatively deep valley network that feeds the canyon that drains to the fan apex (Figure 12a). We use the term "valley" rather than "channel" because the features are much broader and deeper than the channels that cut them. The valleys are cut 80 to 900 m wide and 5 to 110 m deep into the debris mantle. CTX imagery can resolve features on the order of 10 m, but no valley widths smaller than ~80 m were detected, suggesting that the valley network does not continue to extend throughout the entire source area. There is a 291 km^2 eastern portion of the catchment (Figure 12a) that joins the 730 km^2 portion of the catchment through a relatively small valley and at the junction is a partially eroded fan-shaped deposit. This suggests a limited contribution of water and sediment to the 730 km^2 catchment where the valley network has developed.

The main valley that feeds the fan apex ascends across the base of the steep hills defining the back-set crater rim. Tributaries enter from the western upland plains and from the north along the steep hillslopes. The main valley heads up to the east around the back-set hills and forks across the sloping plains in the northern uplands (Figure 12a). A limited but well-developed branching network is established across the northern plains. The total valley length is 107 km, equivalent to a drainage density of 0.15 km/ km^2 for the 730 km^2 area likely contributing water at the time of dissection. Coincidentally, this drainage density value matches the highest valley network drainage densities reported in a global survey by *Hynek et al.* [2010] of over 82,219

valleys, with most of the highest drainage density valleys forming between the latest Noachian and earliest Hesperian epochs. The longitudinal profile from the northern branch of the valley network down to the fan apex (Figure 12b) shows the upland channels to have a slope of 2% or more and that the channel progressively steepens as it descends and enters the main canyon. Here slopes locally reach 10% before the channel exits onto the crater wall and declines to 5%.

The entire incised valley network that leads to Peace Vallis fan is cut into previously accumulated deposits, likely composed of colluvium, fluvial, and eolian debris. Although relatively sharp edged, the incised valleys are floored with dunes and colluvium, indicating they are partially infilled. HiRISE images of the lower part of the main stem valley show boulder-lined banks in some exposures, suggesting mobilization of coarse debris to the fan. Craters 500 m to 1000 m in diameters are partially to mostly infilled, and scour tracks of wind deflation are common. In the limited HiRISE data available some finer-scale infilled channels are visible along the upper crater walls adjacent to the Peace Vallis fan.

5. Sediment Budget

The direct connection of the incised valley network to the fan and the relatively strong morphologic preservation of both the valleys and the fan suggest that the fan sediment is derived from incision of the valley network. Here we test the hypothesis quantitatively by comparing estimates of the eroded and the depositional volumes.

5.1. Volume of Erosion Due To Valley Incision

HiRISE elevation data extend upslope from the fan apex 10 km, and the volume needed to fill the valley in this region can be accurately calculated. Farther upslope, CTX images must be relied upon to estimate eroded volume. For where there is HiRISE coverage, the valley width to incision depth ratio is 18, based on 20 cross sections along the valley. This ratio was used to calculate the depth of erosion for valleys identified in CTX images that lack topographic data to measure depths. The valley network was divided into boxes of uniform width in order to calculate the volume of sediment that had been removed to create that section of the valley. As a test of this box method, the same analysis was done on the lower portion of the Peace Vallis valley network (where HiRISE topographic data are available). Volumes using these high-resolution data were calculated following the methods developed by *Warner et al.* [2011], yielding 0.10 km^3 of material removed from the lower 10 km of the Peace Vallis valley network. The box method gave a similar result of 0.11 km^3. The box method applied to the entire incised valley network gave a volume of 0.8 km^3. This volume is probably an underestimate because the valleys that are partially infilled are not accounted for, nor are smaller valleys that have been erased either through erosion or complete infilling. The estimate also does not account for erosion that occurred outside of the valley network but within the drainage basin.

5.2. Volume of the Fan

Following the methods described in section 2.2, the current volume of the fan is estimated to be 0.7 km^3 (0.5 km^3 for the upper fan and 0.2 km^2 for the lower fan). The different assumptions made about the pre-fan topography result in preserved volumes ranging from 0.4 to 0.8 km^3. For the 0.7 km^3 value, the mean thickness of the fan deposit (for the 80 km^2 fan) is just 9 m. If one reconstructs fan topography (see section 2.2), the amount of wind erosion can be calculated to produce estimates of the original volume of the fan. About 0.14 km^3 has been lost from the lower fan due to wind erosion (Figure 13a). The upper fan has also experienced deflation (hence the paleochannel ridges). For the average depth of 2.4 m of erosion over the entire western fan (25 km^2), a volume of 0.06 km^3 has been removed. The 0.6 m of deflation over the entire eastern fan (55 km^2) equates to 0.03 km^3 of eroded sediment. Hence, the total original fan volume was 0.93 km^3.

5.3. Sediment Budget

Within the error of these estimates, the calculated volume of eroded sediment (0.8 km^3) matches well the volume of the original fan (0.9 km^3). The eroded volume was expected to be an underestimate due to infilling and imperfect preservation of finer valleys. This suggests that the full extent of significant fan deposition has been mapped. This does not rule out transport across Bradbury Rise, but it would argue against the general elevated topography of that rise and of the adjacent broad ridge to the west as originating from deposition of sediment generated from the observed valley incision. Note that since the

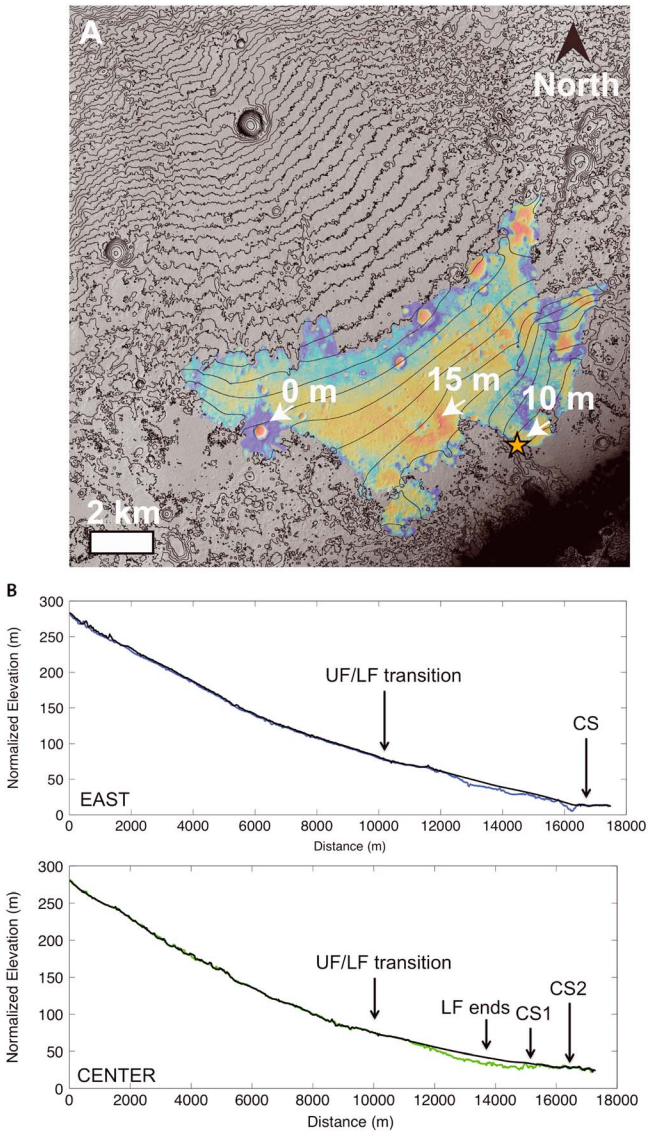

Figure 13. (a) Shown here are 5 m preeroded fan contours that were calculated by projecting a continuation of the current-day upper fan topography to the dark cratered unit to the southeast and other neighboring areas that have experienced minimal erosion. An erosion map was created by differencing the reconstructed fan surface with the current-day fan surface, giving a total erosion volume of 0.14 km^3 from the lower fan and maximum erosion depths of up to 18 m locally. The location of the John Klein drill site [*Grotzinger et al*., 2014] is marked with a star. (b) Reconstructed fan longitudinal profiles (black) are plotted on top of the current-day longitudinal profiles for the eastern (blue) and center (green) fan to show the extent of erosion on the lower fan. The average reconstructed fan slope was calculated every 100 m; and the 10-point average was plotted as a function of distance for the center and east longitudinal profiles in Figure 7c (black).

source material is a granular deposit (not bedrock), the bulk density of the eroded and deposited material was considered the same, such that volumes can be directly compared. The volume agreement also suggests that the valley incision and fan formation were coincident. Gale Crater rim is laced with incised valleys (Figure 3). *Irwin et al*. [2005] proposed that this incision, the associated fan and delta formation, and the possible presence of lakes all occurred in a brief period. Alternatively, lakes, valley incision, and fan and delta formation could have been episodic and not synchronous across Gale. As discussed in the next section, this suggests a need for stronger evidence of the timing of events.

6. Relative Timing

Thompson et al. [2011] proposed that the impact age for Gale, based on crater counts in the surrounding ejecta, occurred in the Late Noachian/Early Hesperian, with uncertainty arising from the occurrence of a few large craters for which it is not clear if they predate or postdate the impact. They counted craters separately on the crater "floor" (which included the crater wall and floor across which the Peace Vallis fan advanced) and concluded that the "floor unit" was also of Early Hesperian age. These counts and stratigraphic relationships suggested to them that the Aeolis Mon deposits were formed soon after impact, about 3.6 to 3.8 billion years ago. They point to the proposal by *Irwin et al*. [2005] that Farah Vallis breached along the south rim and formed two small deposits around what must have been the preexisting mound deposit and conclude that most deposition and channel erosion in Gale Crater occurred in a period of 0.2 to 0.3 Ga post-Gale impact. *Le Deit et al*. [2013], working independently and using only crater counts on the ejecta sheet to the south and east, also arrive at an age of ~3.61 Ga.

Crater counts in the 730 km^2 source area for Peace Vallis fan, much of which lies in the ejecta blanket of Gale, also yielded an age of about 3.6 Ga (M. C. Palucis et al., manuscript in preparation, 2014). This suggests that

the source area has not been resurfaced due to prior erosion and is consistent with the interpretation that the erosion that produced the fan came principally from the observable incised valleys. Early (shortly after impact) erosion and delivery of sediment to the floor of Gale cannot be ruled out. Peace Vallis fan may be too small to obtain reliable crater count age dating directly [e.g., *McEwen and Bierhaus* [2006]; *Michael and Neukum* [2010]], and we see no definitive observations to demonstrate that craters within the fan have preceded the arrival of the relatively thin Peace Vallis fan. *Le Deit et al*. [2013], however, report crater counts for a selected area on the northern crater floor (not including the Peace Vallis fan) that they interpret as suggesting a crater floor age of about 3.4 Ga and then subsequent resurfacing at about 1.1 Ga.

Suggestions of lake development may provide further constraints on Peace Vallis formation timing. Several groups have proposed that after Aeolis Mons formation and its erosion to topography similar to present, lakes formed to various depths [e.g., *Cabrol et al*., 1999; *Irwin et al*., 2005; *Dietrich et al*., 2013; *Le Deit et al*., 2013; and see review in *Anderson and Bell*, 2010]. The deltaic-like forms that have been previously mapped [*Irwin et al*., 2005, Figure 3] as well as fan-shaped deposits at the mouth of the large canyons cut into Aeolis Mons are deposited at elevations far above the Peace Vallis fan. *Anderson and Bell* [2010] documented the canyons on Aeolis Mons, the numerous gullies descending across the crater wall, fan-shaped deposits, and inverted and incised channels that indicated spatially extensive water-driven erosion and deposition processes. If Peace Vallis was active when the other large canyons were depositing sediment, deposition at a similar elevation on the crater wall might be expected (especially if that elevation represents a lake level). Instead, Peace Vallis fan extends to floor of the crater, lower than any other fan-like form. This low position and the apparent lack of post-depositional burial and scour by other events (other than wind erosion) suggest that Peace Vallis fan may be one of the last water-driven depositional events in Gale Crater. Nonetheless, the extensive wind deflation of the lower portion of the fan, the inverted paleochannels on the upper part of the fan, and the generally poorly preserved crater forms on the upper fan all indicate that considerable time has passed since fan formation.

Crater count dating of much larger (~1000 km^2) fans in craters [e.g., *Grant and Wilson*, 2011, 2012] have suggested a possible common development time in the Amazonian. *Mangold et al*. [2012a] concluded, based on crater counts on individual fans in the Margaritifer Terra region, that a late-stage episode of fan construction was Hesperian to early Amazonian in age. *Morgan et al*. [2014] also report fan construction periods of middle to late Hesperian and early Amazonian. Hence, dates elsewhere (on much larger features with more reliable crater counts) point to a timing of Peace Vallis fan (if it were synchronous) as being possibly late Hesperian to early Amazonian.

7. Discussion

Based on the observations reported above, the three key questions can now be explored. Here we find many similarities but some important differences with fans investigated elsewhere on Mars.

7.1. Where Did the Sediment Come From?

The sediment budget analysis strongly suggests that the fan deposits are derived from the visible valley incision into previously deposited debris in the source basin. The origin and process of sediment delivery of this previously deposited debris are less well defined. Most of the sediment in the fan was derived from the wide, deep main stem valley (Figure 12a). This setting would likely favor deposition of coarse debris (including boulders) descending from the adjacent steep valley walls. Debris production could occur by many processes including immediately after the impact (e.g., impact breccia), freeze-thaw activity, or marsquakes. One of the tributaries originating on the steep slopes appears to be marked by parallel-elevated ridges, perhaps levees tracking the path of mass flow deposits to the main stem. Some, if not much, of this sediment may simply be outfall of impact debris and subsequent remobilization from adjacent slopes. The mantling of the hillslopes with fine debris (such that bedrock is rarely visible) points to mobilization, deposition, and perhaps some in situ production of fines. Exposures in the walls of the lower part of the main stem (from HiRISE) show boulders, but the exposures are dominated by sediment finer than boulders. The incised valleys that cut across the plains may have brought finer sediment to the fan, though the 2% valley slope there would still favor gravel-bedded systems.

The main stem canyon may have been a path of water and sediment delivery before Peace Vallis fan formation. The apparent old age of the crater wall adjacent to the fan [*Thomson et al*., 2011], however, does

not suggest significant delivery there, and the reconstructed pre-fan surface would seem to rule out significant deposition from a prior, older fan.

Only two other fans developed within craters on Mars have reported distal light-toned deposits like that found in the Peace Vallis fan. *Mangold et al*. [2012b] noted light-toned, high thermal inertia material distal deposits in Majuro crater. The fan is located in the NE Hellas region and is dated to be late Hesperian by crater counts. It shows small inverted channels in the northern lower section, and phyllosilicates are indicated based on spectral mapping using CRISM data. *Morgan et al*. [2014] observed a distal light-toned deposit in Runanga crater, which is crossed by numerous paleochannels. *Newsom et al*. [2010] documented a light-toned polygonal fractured rock that likely bears Fe/Mg phyllosilicates (also based on CRISM data) on the western floor of Miyamoto crater along with extensive inverted paleochannels, though no fan or delta deposit was observed. Extensive wind deflation of fans has been documented elsewhere [e.g., *Morgan et al*., 2014] suggesting fine-grained deposition is prevalent, but the presence of the light-toned fractured pattern may occur only with significant hydrothermal alteration, as suggested by *Newsom et al*. [2010] and *Mangold et al*. [2012b]. Investigations resulting from the *Curiosity* rover investigations may provide constraints on the origin of the fracturing and what that implies about source material and post-depositional processes.

7.2. What Processes Formed the Fan?

The processes of sediment delivery to the fan and transport across it, and net deposition appear to differ spatially and, perhaps, through time. The main stem valley that feeds the fan originates in tributaries lying in 2% sloping valleys in broad upland plains. Channels on 2% slopes likely carried mixtures of sand, gravel, and boulders and may well have been braided. Given the distance to any steep slopes, it is unlikely that mass transport events (e.g., mudflows) occurred in these upland channels. However, as the upland channels collected and drained into the main stem from the northeast, the convex profile progressively steepened (Figure 12b) to local reaches of 10% and an average slope of 8%. This is a very steep slope for such a large drainage area (730 km^2), which means that flows through these valleys were capable of producing shear stresses of exceptional magnitude for relatively modest discharges. Such flows likely caused rapid channel incision into finer material until slowed by bedrock resistance or large grains. Current burial by colluvium and eolian deposits and insufficient HiRISE coverage at the time of this publication prevents evaluation of the bed conditions. However, the preservation of such a steep main stem suggests limited water runoff, as sustained flow would cause incision that would tend to drive the form to concave up and advance the steep reach into the upland plains. In the local steep tributaries, debris flows or mudflows may have been generated, traveling into the main stem. Such a steep main stem channel would have transported these flows to the fan. Within the source area channels, sediment could have traveled up to 35 km before reaching the fan, providing ample travel distance to round sediment and breakdown weak material.

Runoff that drove valley incision in the source area could be due to groundwater flow, rainfall, or snowmelt. Groundwater discharge is unlikely as a source mechanism for runoff based on the geometry of the channels and the channel network. The channel tips in the uplands originate in broad plains with distant hills rising typically less than 350 m above the surrounding topography. On the steep tributaries along the main stem, the channels extend well up the hills. However, none of the channel heads take the characteristic amphitheater shape associated with seepage erosion in loose material, and the valley network is a branching system, not a single unbranched valley, which is typical of groundwater discharge [e.g., *Laity and Malin*, 1985]. All of these observations argue against groundwater flow as a runoff generation mechanism. This leaves runoff from rain or snow. Snow could accumulate in the uplands and funnel water to the fan upon melting. Rain would likely occur over a larger regional scale, perhaps across the entire crater rim, but there is no evidence of preserved extensive channel networks to confirm that rainfall was the dominant source of water for fan formation (although incised valleys do ring the crater wall) (Figure 3). The Hesperian to Amazonian age of the fan may make rain less likely as both the atmospheric pressure and temperature are thought to be too low to support rainfall [*Forget et al*., 2013; *Woodsworth et al*., 2013], though *Craddock and Howard* [2002] suggest that the morphology and drainage density of highland valley networks point to rainfall occurring possibly into the Amazonian. Hence, we propose, as others have done for fans across Mars [e.g., *Howard and Moore*, 2011; *Grant and Wilson*, 2012; *Mangold et al*., 2012c; *Morgan et al*., 2014], that runoff was more likely dominated by snowmelt. A terrestrial

analog would be the McMurdo Dry Valleys, in which most precipitation falls as snowfall (though small amounts of rainfall have been known to occur in the summer) and channelized ephemeral streams are sourced completely from meltwater [*Conovitz et al*., 1998; *Fountain et al*., 1999].

Once runoff and the sediment it carried reached the fan, sediment transport likely occurred by several mechanisms. Clearly, fluvial channel-bound processes occurred, as evidenced by the numerous paleochannels. The elevated channel beds (now ridges) indicate that finer-grained overbank sediments in flood flows, capable of being swept away by wind, must have also been deposited. Boulder abundances associated with the paleochannels may decrease downslope. Although, it is often assumed that grain size decreases down alluvial fans, as *Stock et al*. [2008] and *Stock* [2012] report in their review of fan processes, that it is often not the case on terrestrial fans. Sheet floods may have also occurred across the fan where relatively dilute flows spill out of channels and travel across the fan, causing both scour and deposition. Lastly, mudflows could have traveled the entire length of the fan if sufficient fines of sand, silt, and clay were present to generate them. We see no morphologic evidence of mudflow processes, but such evidence may be subtle. *Morgan et al*. [2014] describe mudflows in relatively low-gradient fans in the Atacama Desert. These flows travel down channels on the fan, exceed the channel carrying capacity, and then spill out across the fan surface for a considerable distance. This would be difficult to detect using HiRISE data.

The transition from the upper fan, where the channels are presumably armored against significant deflation by pebbles and gravel, to the channel-less lower fan, suggests that although gravel units may occur in the lower fan, the gravel abundance is not sufficient to form a protective armor. The absence of elevated channel paths in the lower fan may be due to either the channels being sand-bedded and thus incapable of armoring against wind deflation or that channelized flow was absent and instead sheetflood transport conditions prevailed. We note that the lower portion of the fan descends into an enclosed topographic basin (Figure 5a), suggesting the lower fan may have periodically encountered a shallow lacustrine environment. Direct observations of the lower fan deposits in Yellowknife Bay indicate the presence of laterally extensive mudstones indicating lake sediments [*Grotzinger et al*., 2014].

Nearly all other Martian fans are characterized by a radial pattern of distributary channels exposed as ridges across the fan [*Moore and Howard*, 2005; *Morgan et al*., 2014]. The absence of paleochannels for much of the eastern portion of the upper fan, yet the apparent lack of deep wind deflation, suggests that flows on the eastern part of the fan were either not channelized or the interchannel sediments were coarser grained and harder to deflate. If the former occurred, one possibility is that the flows that crossed and built the eastern portion of the fan, and deposited much of the finer-grained light-toned unit of the lower fan, were smaller in magnitude and simply spilled and spread as episodic patchy sheet floods across the fan. Terrestrial fans often lack well-defined continuous channel systems, and we know from observations at Yellowknife Bay [*Grotzinger et al*., 2014] that the lower fan could be a mixture of fluvial and shallow lacustrine deposits. Consistent with this sheetflood hypothesis is the presence of pebble conglomerate outcrops across Bradbury Rise [*Williams et al*., 2013a]. These deposits may record the transport of gravels from the Peace Vallis fan toward Aeolis Mons. No channel paths or elevated channel beds have been detected here, and the absence may reflect sheetflood transport processes.

To assess how much runoff may have been involved in building a depositional feature like the Peace Vallis fan, the common practice has been either to assume a water to rock ratio [*Mangold et al*., 2012c] or to perform a hydraulic analysis based on estimated channel and grain size characteristics to calculate channel filling flows [e.g., *Wilson et al*., 2004]. Both approaches are very approximate. Typical rock/water ratios vary by orders of magnitude and depend on grain size and climate characteristics. The hydraulic calculations require many assumptions that cannot be tested and only provide instantaneous discharge estimates. Perhaps the most relevant terrestrial study in providing an estimate of rock/water ratios for the Peace Vallis fan system is the work by *Pepin et al*. [2010] across Chile. They analyzed the suspended sediment annual yield as a function of mean annual runoff. For low-vegetation density in very dry regions, the annual rock/water ratio was about 0.0002. For a fan sediment volume of 0.93 km^3, the ratio suggests that 4650 km^3 of water runoff would be needed. This is equal to about 6 km of water across the active catchment. *Syvitski et al*. [2003] collected runoff and sediment flux data for 340 terrestrial river basins around the world, and the log transformed rock/water ratio yields a roughly Gaussian curve with a mean value of 0.0001 ± 0.00008. The estimate of the rock/water ratio on Mars to drive fluvial sediments at other locations has varied greatly. For example, *Moore et al*. [2003]

assume 0.05. *Mangold et al*. [2012c] proposed 0.0005 for dilute flows and 0.02 to 0.3 for dense flows. *Morgan et al*. [2014] chose a concentration of 0.2, reflecting the inference that the fans in Saheki crater were built in large part by mudflows. The very conservative 0.2 concentration applied to the Peace Vallis fan would still require 6 m of water to be produced over an area of 730 km^2 in the active catchment. The observations of fluvial gravels reported in *Williams et al*. [2013a] across Bradbury Rise, however, show that dilute transport did occur and the effective concentration would be well below 0.2. Drilling by the *Curiosity* rover into the light-toned unit revealed a mudstone (i.e., Sheepbed member) that likely extends at least 4 km^2 and records a lacustrine environment that may have persisted for hundreds to thousands of years [*Grotzinger et al*., 2014]. Considering the extent of exposure of what appears to be fluvial/lacustrine deposits in the lower fan, *Grotzinger et al*. [2014] hypothesize the sediments could have been deposited over millions of years. The abundant evidence of sorted sediments and lacustrine deposits strongly suggests that the more likely rock to water ratio is closer to that observed in Chile (i.e., 0.0002) or even the global average on Earth (0.0001). Conservatively selecting 1 order of magnitude higher concentration than the Chilean value still requires about 600 m of runoff from the 730 km^2 source basin (i.e., 465 km^3 of water). This hydrologic analysis supports the sedimentologic inference by *Grotzinger et al*. [2014] that the fan was active over an extended period of time, and it requires the establishment of a hydrologic cycle (rather than a single melt event) to generate this large amount of runoff.

Another constraint on runoff is to estimate the instantaneous discharge in a paleochannel crossing the fan [e.g., *Wilson et al*., 2004; *Williams et al*., 2009b; 2013a; *Morgan et al*., 2014]. We use standard hydraulic equations and threshold channel concepts along with slope data and our measurements of channel width to determine the likely grain sizes that comprised the channel bed and the instantaneous discharges and flow velocities at bankfull conditions for a "representative" cross section.

The fluid discharge, Q, within a channel can be derived by conservation of mass,

$$Q = uhw \tag{1}$$

where u is the average flow velocity, h is the channel depth, and w is the channel width. For channels with width-to-depth ratios less than 20, the hydraulic radius, R, which is the ratio of the channel area to its wetted perimeter, is used instead of h. For a turbulent velocity profile (i.e., Reynold's number, Re_{channel}, is > 1000 [*Chow*, 1964]), the velocity, u, is found at a given height above the bed, z, using the law of the wall formulation,

$$u = \left(\frac{u_*}{k}\right) ln\left(\frac{z}{z_o}\right) \tag{2}$$

where z_o is the roughness coefficient, k is the dimensionless von Karman's constant (typically 0.41 [e.g., *Furbish*, 1997; *Garcia*, 2008]), and u_* is the shear velocity, defined as

$$u_* = \left(\frac{\tau_b}{\rho}\right)^{0.5}. \tag{3}$$

In equation (3), τ_b is the boundary shear stress, defined as

$$\tau_b = \rho ghS, \tag{4}$$

where ρ is the fluid density, g is the gravitational constant (3.711 m/s^2 for Mars), and S is water surface slope (assumed to equal measured topographic slope in this analysis). The roughness coefficient for hydraulically rough flow is

$$z_o = \frac{k_s}{30}, \tag{5}$$

where 30 is the Nikuradse roughness coefficient and k_s is the effective roughness height, typically approximated as $k_s = 3.5\ D_{84}$, [e.g., *Garcia*, 2008] giving

$$z_o = \frac{3.5}{30} D_{84}. \tag{6}$$

The vertically averaged velocity is

$$\overline{u} = \frac{u_*}{k} ln\left(\frac{11h}{3.5D_{84}}\right), \tag{7}$$

where the 11 in equation (7) is the result of integrating the log profile constant and multiplying it by the Nikuradse roughness (i.e., 30). Assuming that the boundary shear stress needed to move the median grain size on the bed (D_{50}) is the critical boundary shear stress [e.g., *Buffington and Montgomery*, 1997],

$$\tau*_{cr} = \frac{\rho g h S}{(\rho_s - \rho) g D_{50}}, \tag{8}$$

(ρ_s is the sediment density) and the shear velocity, u_* is

$$u_* = \left(\tau*_{cr} \frac{(\rho_s - \rho)}{\rho} g D_{50}\right)^{0.5}. \tag{9}$$

Vertically average velocities reported here are derived from equation (7) and the relationship given for shear velocity given in equation (9). Instantaneous discharge is then calculated from equation (1).

The average paleochannel bed width on the western fan is 27 m. Channel slope is set to 0.01 and 0.02 (the steeper slope is more characteristic of where the channel widths were measured). Martian gravity is 3.711 m/s^2, the sediment density is 3000 kg/m^3 (typical of basalt), and fluid density of 1000 kg/m^3 (low concentration flow). We assume a range of critical shear stresses, $\tau*_{cr}$, from 0.02 (for sandier beds) to 0.06 (for coarser beds) [e.g., *Parker et al*., 1998; *Parker*, 2008; *Garcia*, 2008] and a range of width-to-depth ratios to determine the mobile median grain size under critical conditions by rearranging equation (8) to solve for D_{50}. To constrain the likely grain size in the channels on Peace Vallis fan, we assume width-to-depth ratios between 10 and 100, which are the range of aspect ratios observed for terrestrial alluvial rivers [*Knighton*, 1998] and for channels on several arid to semiarid alluvial fans [*Stock et al*., 2008]. Given the possible braided form in the western portion of the fan, a value closer to 100 is more likely. The roughness length scale D_{84} is set equal $1.5D_{50}$ [*Morgan et al*., 2014]. Also, when the width-depth ratio is less than 20, the hydraulic radius, R, is used in place of channel depth, h. As a separate constraint, flow is also assumed to be critical, i.e., the Froude number is 1, which has been observed on terrestrial fans (see review in *Stock* [2012]).

The predicted grain size for the western fan paleochannels of 2% slope lies in the gravel to boulder range (Figure 14). For a given flow depth (i.e., W/h) the lower critical Shields number predicts a larger grain size. Predicted grain size is proportional to slope, so for a given flow depth, if the slope were 1% the predicted values would all decrease by a factor of 2 but still remain in the gravel to boulder-size range. Given the possible braided channel state (with a high W/h) and the lack of abundant boulders visible on HiRISE, the likely median bed surface grain size is probably closer to the low value of 45 mm for the 0.06 critical Shields number. An independent check, which assumes a critical flow depth ($Fr = 1$), predicts a still smaller median grain size of 30 mm at a W/h of 100. Data from an analog fan in the Atacama Desert (Chile) [*Morgan et al*., 2014] lie along the $Fr = 1$ line, supporting its use in this analysis. For W/h of 100 and a slope of 2% for the paleochannels on the western fan, the predicted flow velocity ranges from 0.5 to 0.9 m/s for low to high critical Shield numbers respectively. This equates to instantaneous discharges of 3.7 to 6.5 m^3/s. If the channels were much deeper, i.e., W/h of 10, the velocities would climb to 1.6 to 2.8 m/s, respectively, and the discharges would be 117 m^3/s to 207 m^3/s.

For the Peace Vallis catchment area of 730 km^2, these discharges require water supply rates between 0.02 mm/h (high W/h) and 1 mm/h (low W/h), which assumes the entire catchment simultaneously melts and produces a steady runoff rate. During any flow event, there may have been more than one channel on the fan receiving flow, so discharge may have been higher. These input estimates are also conservative, as they assume no losses due to refreezing, evaporation, or infiltration. If we assume these losses to be relatively minor, then input rates need to be sustained on a timescale comparable to that needed for water to travel through the valley network (length ~50 km). Assuming flow velocities on the fan are comparable to velocities in the incised valley network, flow would need to be sustained between 5 (high W/h) and 27 (low W/h) h in the headwaters.

Based on geomorphic evidence and the likely deposition of the fan in the Hesperian or Amazonian, we assume discharges could have been generated by snowmelt. Global climate models show that snow accumulation is possible in the equatorial highlands of Mars, assuming a faint young Sun and a denser CO_2 atmosphere [e.g., *Woodsworth et al*., 2013; *Kite et al*., 2013]. *Williams et al*. [2008, 2009a, 2009b] use a snowpack model to show that for the past 5 Ma, latitudes between 70°N and 70°S correspond to significant seasonal snowmelt runoff

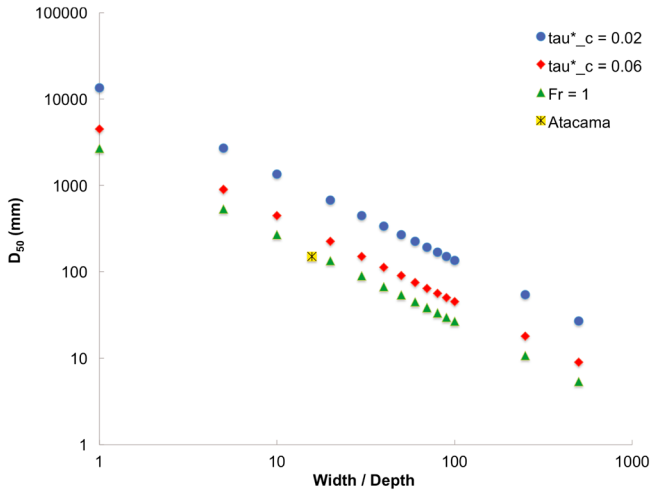

Figure 14. Using threshold channel concepts, the median grain size on a 2% channel bed (D_{50}) for given width to depth ratios (W/D) under typical critical shear stresses (defined as the shear stress over the grain weight) is plotted for sandy ($\tau_{cr} = 0.02$) to gravelly beds ($\tau_{cr} = 0.06$). Using the constraints that terrestrial alluvial channels typically have W/D ratios between 10 and 100, and Froude (*Fr*) numbers close to 1 [*Stock et al.*, 2008], Peace Vallis fan would likely have transported gravel to possibly boulder-sized material. Pebble count data from a terrestrial analog fan in the Atacama Desert (Chile), which also has a mean slope of 1.5%, falls within the predicted ranges for Peace Vallis fan.

(>1 mm) on the order of several days a year. *Kite et al.* [2013] suggest that over Mars' history, peak snowmelt rates were likely between 2 and 3 mm/h, which is adequate to drive the highest estimated discharges and are well above the more probable lower values. The topography of the Peace Vallis source area (Figure 11a), where large plains are bordered by hills, appears particularly well suited to collect snow and release snowmelt.

7.3. How Did the Fan Evolve?

Here we use the observations reported above to propose a possible evolutionary history of Peace Vallis fan. It is hoped that this hypothesis may eventually be explored through modeling. The initial conditions for Peace Vallis formation appear to be an established large uplands catchment variably mantled in debris, a concave up south facing crater wall (lacking a prominent prior fan form), and a complex crater floor consisting of a broad relatively flat ridge, a rise and a low (Figures 11a and 6b). Runoff, possibly due to snowmelt, would follow the maximum fall path and concentrate along the steep canyon, cutting into the accumulated debris. Permeability of this debris would influence how much surface runoff would be generated and the resulting valley incision. The developing channel system would expand along the topographic convergent areas through the uplands, down the steep canyon, and onto the crater wall. As the channel cut across the lower wall, it took a diagonal path. When the main valley opened up into the crater, sediment-depositing flows likely first headed down the maximum fall direction along the eventual western margin of the fan. Hence, the channel-rich western fan may have been the first path of deposition.

If flow was limited in duration or peak volume, the fan may have advanced episodically down the relatively gently sloped crater wall leaving patches of coarse material bordered by finer-grained sediment and perhaps local playa lake deposits in enclosed lows. Alternatively, sufficient flows may have produced continuous channels across the fan to the crater floor. In this case, the fan form may have advanced upslope from the lower topographic boundary condition. Clearly, such channels did eventually develop as evidenced by the numerous preserved paleochannel beds in the western fan. These channels do not radiate or show signs of a distributary behavior and instead may record a period of braided channel transport conditions along the western fan. Overbank events would spread finer sediment across adjacent plains that subsequently would be subjected to deflation, leaving gravel-bedded channel paths elevated.

Aggradation causes epicenters of fan deposition to shift, and the hypothesized initial deposition along the western margin would cause the fan construction to shift eastward. This proposed time sequence suggests that the mode of transport changed from significant channelized flow and sediment transport to more dispersed possible sheetflood transport. Small discontinuous gravel-bedded channels (a few meters across) could transit this area, but deflation would not preserve the channel traces. The transition from the upper fan's coarse mantle material to the fine-grained, fractured lower fan deposits [*Sumner et al.*, 2013] occurs where the slope declines to 1% (at about 10 km from the apex) (Figure 7c). Although still relatively steep, this slope reduction may favor spreading of the flows, transition from suspension to bed load transport of sand, and a predominance of sand and finer sediment deposition in general. These changes in sedimentation style may have caused the change in surface properties from mottled exposures in the upper fan to the

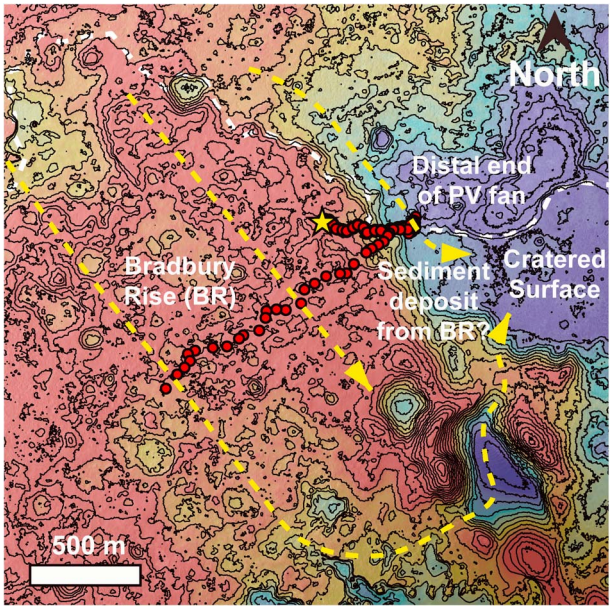

Figure 15. Colored elevation map with 2 m delta radii HiRISE contours overlaid. For reference, there is a 17 m difference between the elevation on Bradbury Rise and the eroded portion of the lower fan. The star marks Bradbury Landing, and the red dots mark stops along the rover traverse during the first 360 Martian solar days. The yellow dashed lines show possible paleoflow lines across Bradbury Rise and/or onto the cratered surface, creating what is possibly a small fanlike feature as sediment was deposited off of Bradbury Rise.

light-toned outcrops with scarps and higher thermal inertia characteristic of the lower fan. Patches of gravel associated with discontinuous channels may still have formed on the lower fan but not enough to later prevent deflation. Below the transition, the fan descended into an enclosed basin and down to a local topographic low where the fan form terminates (Figure 11a). Given this topography and the distal position on the fan, lake conditions may have developed.

The center part of the fan likely prograded onto Bradbury Rise, and the sediment transported in these flows would possibly continue downslope toward Aeolis Mons (Figure 15). If this occurred, the gravels reported by *Williams et al.* [2013a] may be a record of this process. It is possible that some of these flows spilled off Bradbury Rise onto the local cratered surface, creating a local fan-shaped deposit. Detailed mapping is still being done to assess whether the sands and gravels of the Bradbury Rise area are best considered ancient (preceding the fan) or derived from it directly.

There are distinct topographic components to the fan with different focal locations associated with distinct sets of arc-shaped contours (Figure 5c). Only the lowermost convex contours appear to define a continuous topographic feature across the entire fan. Although these different components grade smoothly into each other, they may record variations in both space and time of fan development. The thin beds of sediment visible in HiRISE data in the lower fan, the numerous paleochannels, and the topographic complexity of the fan all suggest that hundreds to thousands of flow events were needed to build the fan.

Even the most conservative of estimates requires at least 600 m of water over the 730 km^2 active source area to build Peace Vallis fan (i.e., ~500 km^3 of water). Likely, much more water was involved, possibly in excess of 1000 km^3. This requires a hydrologic cycle and considerable time. This is consistent with the inferences obtained from the sedimentology and stratigraphy revealed by the *Curiosity* rover [*Grotzinger et al.*, 2014]. In a study of larger equatorial fans on Mars, *Moore and Howard* [2005] concluded that construction took tens of thousands to hundreds of thousands (perhaps millions) of years, a conclusion recently reinforced by *Armitage et al.* [2011]. Our smaller fan may fall toward the shorter time period of this estimate, but that depends on how intermittent the favorable climate conditions were.

Post-fan deflation occurred across the entire fan but was greatest in the light-toned fractured lower fan. On the western fan, 2.4 m of erosion is needed to elevate the paleochannels, and if we estimate a younger age of the fan to be 2 Ga, then this indicates an erosion rate of 1 to 5 nm/yr, whereas the eastern upper fan eroded 0.6 m or 0.3 to 1.2 nm/yr. The amount of erosion is highly variable in the lower fan (Figure 13a). The average is 5 m, but locally it exceeds 10 m. This corresponds to an erosion rate low of 2.5 nm/yr (over 2 billion years) to a local high to 20 nm/yr (10 m/500 million years). *Farley et al.* [2014] estimate local wind-driven scarp retreat, based on surface exposure age dating of 0.75 m/million years and suggest from this that wind erosion may be episodic in Gale. Other than wind deflation, we have found no evidence of further fan evolution. Others have suggested that fan construction abruptly halted on Mars [i.e., *Moore and Howard*, 2005]. Our observations do not contradict this inference.

One possible time sequence of events in Gale Crater is: impact, center mound infill and scour, multiple lake and associated fan and delta formation (Figure 3), and ultimately, the Peace Vallis fan formation. The timing of the numerous incised valleys and downslope paleochannels in Gale Crater (Figure 3) remains uncertain. Further work is needed to establish the relative timing of these valleys and channels. This matters to constraining further the necessary climatic conditions that led to the formation of the Peace Vallis fan.

This analysis of Peace Vallis fan formation differs in some ways from that proposed by *Anderson and Bell* [2010]. They propose that the light-toned fractured deposit (their high thermal inertia fan-shaped unit) is a relatively thick deposit that underlies the crater floor and that the "low thermal inertia unit" is a thin overlying mantle [*Anderson and Bell*, 2010, Figure 47]. They point to fractures in the low thermal inertial unit as evidence of a thin mantle that transmits the fractures. Fractures in the low thermal inertia unit are not strongly developed, and crater walls in the upper fan (low thermal inertia unit) do not show the fractured, resistant material. More importantly, *Sumner et al.* [2013] show the transition from upper to lower fan to be gradational and intermixed.

8. Summary

The Peace Vallis fan is defined by convex contours that extend across the lower portion of the northern Gale Crater wall and terminate at the topographically diverse floor at the base of Aeolis Mons. Covering about 80 km^2, the upper portion of the fan is a relatively fracture-free, mottled surface and is laced on its western margin with frequent ridges interpreted to be paleochannel beds. The lower portion of the fan has high thermal inertia compared to the upper portion, is light toned, and generally highly fractured. This lower portion is deflated locally up to 15 m, indicating that it is at least partially composed of finer sediment that is capable of being swept away by wind. The fan also varies laterally from a western side that slopes primarily to the south and contains the paleochannels and an eastern side that slopes toward the southeast and has only a few low-relief paleochannels. The western portion of the fan terminates on a broad, nearly flat ridge that extends across from Aeolis Mons to the crater wall. The eastern portion of the fan may have prograded onto and possibly across the preexisting Bradbury Rise (the *Curiosity* rover landing area) and descended to a topographic low to the east of Bradbury Rise. The longitudinal profile of the fan progressively declines in slope from about 3% at the fan apex to 1% or less where the fan progrades across preexisting topography. The eastern portion of the fan enters an enclosed basin, leading to the prediction that the distal end of the eastern fan included lake deposits, which was subsequently demonstrated by observations obtained by the *Curiosity* rover [*Grotzinger et al.*, 2014].

The location of the Peace Vallis fan results from a 15 km setback in the crater rim, which enables drainage from the adjacent plains near the crater rim to spill into a canyon where an incised valley feeds the apex of the fan. A catchment area up to 1021 km^2 could have fed the valley. The entire incised valley network that fed the fan with water and sediment appears to be excavated into previously deposited debris, likely of colluvial (i.e., mass transport), eolian, fluvial, and possibly air fall origin. Estimates of volume removed to form the incised valley (0.8 km^3) match the total volume of the original fan (0.9 km^3). This suggests that the fan records a distinct episode of valley incision and fan development. Given the preservation of the sharp incised valley walls and fan topography, no further water-driven processes have modified these features (but wind transport has actively eroded fine-grained material and infilled craters).

The gradient of the upland plains valley networks (~2%) and their considerable distance from steep adjacent slopes in the canyon indicate that incision here was driven by fluvial transport, likely in gravel-bedded channels. The main canyon valley and its adjacent tributaries are much steeper, and locally, the main stem approaches 10%. Here mass flows may have originated and carried sediment down to the fan. The progressive decline in fan gradient, an apparent reduction in boulder abundance, the preservation of braided paleochannels in the western portion of the fan, and the transition to actively wind deflated (and thus finer grained) laterally extensive beds all point to a predominance of fluvial transport in fan construction. Given the low ratio of sediment volume to water volume that typifies the fluvial transport of sand and coarser materials, fan construction would require at least 600 km^3 and perhaps more than 6000 m of runoff from the 730 km^2 watershed. As others have concluded for similar fans on crater walls on Mars, the construction period must have taken at least thousands of years if not much longer [*Grotzinger et al.*, 2014].

The source of water for valley incision and Peace Vallis fan development is suggested by the following observations: (1) the valley system, which does form a branching network, is of limited extent (drainage density is about 0.15 km/km^2), (2) the channel tips originate either in broad inclined plains in the uplands or on steep hillslopes, and the tips do not form amphitheater headwalls, (3) a large volume of water is needed to deposit the fan ($>$1000 km^3), and (4) valley incision occurred after Gale impact at about 3.6 Ga. The geomorphic features of the valley network, the lack of a large elevated source area, and the requirement of a large volume of water make groundwater flow an unlikely water source. The lack of channel networks below the source area (that might record runoff from rainfall) and the age of the Gale impact suggest that snow accumulation and melting is a probable explanation for the dominant water source. The large amount of water needed to build the fan requires there to be, however, a hydrologic cycle.

The Peace Vallis fan provides a framework for predicting stratigraphy and potentially habitable environments. With regards to observations by the *Curiosity* rover, the sediments associated with the fan were derived from previously deposited debris, not directly from erosion of bedrock. This adds an extra step in exploring the controls on sediment composition as influenced by weathering and transport. The enduring activity for thousands of years for fan development, similar to that reported elsewhere for fans on crater walls, forces an examination of how climate conditions could develop to create a persistent hydrologic cycle of water storage, runoff, and erosion. The fan crossed a preexisting low-gradient crater wall and floor, and its topographic form suggests that it may have on-lapped preexisting topography at its distal margins. The origin of this preexisiting topography, like the accretion of debris on the Gale walls and the generation of local ridges, rises, and basins, is not yet explained. Further clues may well come from what lies in the exposures awaiting *Curiosity* at the base of Aeolis Mons.

Acknowledgments

This research was conducted for the Jet Propulsion Laboratory, California Institute of Technology, under a contract with NASA under the Mars Program Office. We would like to thank Alan Howard, the entire MSL team, but especially John Grotzinger, Bernard Hallet, Ron Sletten, and Mike Malin for insightful discussions along the way. We greatly appreciate the comments and suggestions provided by our reviewers, especially those from Bob Craddock. We also thank the teams responsible for the orbital data, namely, the HiRISE, CTX, and HRSC teams. We give special thanks to Malin Space Science Systems, the USGS at Flagstaff, and Scott Mansfield, Jonathan Joseph, and Thomas Gautier from Cornell for image and data processing.

References

Anderson, R. B., and J. F. Bell III (2010), Geologic mapping and characterization of Gale Crater and implications for its potential as a Mars Science Laboratory landing site, *Mars*, *5*, 76–128, doi:10.1555/mars.2010.0004.

Armitage, J. J., N. H. Warner, K. Goddard, and S. Gupta (2011), Timescales of alluvial fan development by precipitation on Mars, *Geophys. Res. Lett.*, *38*, L17203, doi:10.1029/2011GL048907.

Buffington, J. M., and D. R. Montgomery (1997), A systematic analysis of eight decades of incipient motion studies, with special reference to gravel-bedded rivers, *Water Resour. Res.*, *33*(8), 1993–2029.

Cabrol, N. A., E. A. Grin, H. E. Newsom, R. Landheim, and C. P. McKay (1999), Hydrogeologic evolution of Gale Crater and its relevance to the exobiological exploration of Mars, *Icarus*, *139*(2), 235–245, doi:10.1006/icar.1999.6099.

Chaytor, J. D., U. S. ten Brink, A. R. Solow, and B. D. Andrews (2009), Size distributions of submarine landslides along the U.S. Atlantic margin, *Mar. Geol.*, *264*, 16–27.

Chow, V. T. (1964), *Open-Channel Hydraulics*, McGraw Hill Book Company, Inc., Caldwell, N. J.

Clarke, J. D. A., and C. R. Stoker (2011), Concretions in exhumed and inverted channels near Hanksville Utah: Implications for Mars, *Int. J. Astrobiol.*, *10*(3), 161–175, doi:10.1017/S1473550411000048.

Conovitz, P. A., D. M. McKnight, L. M. McDonald, A. G. Fountain, and H. R. House (1998), Hydrologic processes influencing streamflow variations in Fryxell Basin, Antarctica, in *Ecosystem Dynamics in a Polar Desert, The McMurdo Dry Valleys, Antarctica*, Antarctic Research Series, vol. 72, edited by J. C. Priscu, pp. 93–108, AGU, Washington, D. C.

Craddock, R. A., and A. D. Howard (2002), The case for rainfall on a warm, wet early Mars, *J. Geophys. Res.*, *107*(E11), 5111, doi:10.1029/2001JE001505.

Dietrich, W. E., T. Parker, D. Y. Sumner, A. Hayes, M. C. Palucis, R. M. E. Williams, F. Calef, and the MSL team (2013), Topographic evidence for Lakes in Gale Crater, Lunar and Planetary Sci. Conf. XLIV, Abstract 1844.

Farley, K. A., et al. (2014), In situ radiometric and exposure dating of the Martian surface, *Science*, *343*, doi:10.1126/science.1247166.

Forget, F., R. Wordsworth, E. Millour, J. B. Madeleine, L. Kerber, E. Marcq, and R. M. Haberle (2013), 3D Modeling of the early Martian climate under a denser CO_2 atmosphere: Temperatures and CO_2 ice clouds, *Icarus*, *222*, 81–99.

Fountain, A. G., et al. (1999), Physical controls on the Taylor Valley Ecosystem, Antarctica, *BioScience*, *49*(12), 961–971.

Furbish, D. J. (1997), *Fluid Physics in Geology*, pp. 476, Oxford Univ. Press, New York, N. Y.

Garcia, M. H. (2008), *In Sedimentation Engineering: Processes, Measurements, Modeling, and Practice*, vol. 110, edited by M. H. Garcia, pp. 165–251, American Society of Civil Engineers, Reston, Va.

Golombek, M. P., et al. (2012), Selection of the Mars Science Laboratory landing site, *Space Sci. Rev.*, doi:10.1007/s11214-012-9916-y.

Grant, J. A., and S. A. Wilson (2011), Late alluvial fan formation in southern Margaritifer Terra, Mars, *Geophys. Res. Lett.*, *38*, L08201, doi:10.1029/2011GL046844.

Grant, J. A., and S. A. Wilson (2012), A possible synoptic source of water for alluvial fan formation in Southern Margaritifer Terra, Mars, *Planet. Space Sci.*, *72*(1), 44–52.

Grotzinger, J. P., et al. (2014), A habitable fluvio-lacustrine at Yellowknife Bay, Gale Crater, Mars, *Science*, *343*, doi:10.1126/science.1242777.

Hallet, B., R. S. Sletten, W. Stewart, R. W. E. Williams, N. Mangold, J. Schieber, D. Sumner, G. Kocurek, and the MSL team (2013), *Fracture Networks, Gale Crater*, Lunar and Planetary Sci. Conf. XLIV, Abstract 3108.

Howard, A. D., and J. M. Moore (2011), Late Hesperian to early Amazonian midlatitude Martian Valleys: Evidence from Newton and Gorgonum Basins, *J. Geophys. Res.*, *116*, E05003, doi:10.1029/2010JE003782.

Hynek, B. M., M. Breach, and M. R. T. Hoke (2010), Updated global map of Martian valley networks and implications for climate and hydrologic processes, *J. Geophys. Res.*, *115*, E09008, doi:10.1029/2009JE003548.

Irwin, R. P., A. D. Howard, R. A. Craddock, and J. M. Moore (2005), An intense terminal epoch of widespread fluvial activity on early Mars: 2. Increased runoff and paleolake development, *J. Geophys. Res.*, *110*, E12S15, doi:10.1029/2005JE002460.

Kite, E. S., I. Harvey, M. A. Kahre, M. J. Wolff, and M. Manga (2013), Seasonal melting and the formation of sedimentary rocks on Mars, with predictions for the Gale Crater mound, *Icarus*, *223*, 131–210, doi:10.1016/j.icarus.2012.11.034.

Knighton, D. (1998), *Fluvial Forms and Processes: A New Perspective*, Oxford Univ. Press Inc., New York, N. Y.

Kraal, E. R., E. Asphaug, J. M. Moore, A. Howard, and A. Bredt (2008), Catalogue of large alluvial fans in Martian impact craters, *Icarus*, *194*, 101–110.

Laity, J. E., and M. C. Malin (1985), Sapping processes and the development of theater-headed valley networks on the Colorado Plateau, *Geol. Soc. Am. Bull.*, *92*(2), 203–217, doi:10.1130/0016-7606.

Le Deit, L., E. Hauber, F. Fueten, M. Pondrelli, A. Rossi, and R. Jaumann (2013), Sequence of infilling events in Gale Crater, Mars: Results from morphology, stratigraphy, and mineralogy, *J. Geophys. Res. Planets*, 2439–2473, doi:10.1002/2012JE004322.

Malin, M. C., and K. S. Edgett (2000), Sedimentary rocks on early Mars, *Science*, *290*, 1927–1937, doi:10.1126/science.290.5498.1927.

Mangold, N., S. Adeli, S. Conway, V. Ansan, and B. Langlais (2012a), A chronology of early Mars climatic evolution from impact crater degradation, *J. Geophys. Res.*, *117*, E04003, doi:10.1029/2011JE004005.

Mangold, N., J. Carter, F. Poulet, E. Dehouck, V. Ansan, and D. Loizeau (2012b), Late Hesperian aqueous alteration at Majuro crater, Mars, *Planet. Space Sci.*, *72*(1), 18–30, doi:10.1016/j.pss.2012.03.014.

Mangold, N., E. S. Kite, M. G. Kleinhaus, H. Newsom, V. Ansan, E. Hauber, E. Kraal, C. Quantin, and K. Tanaka (2012c), The origin and timing of fluvial activity at Eberswalde crater, Mars, *Icarus*, *220*(2), 530–551, doi:10.1016/j.icarus.2012.05.026.

McEwen, A. S., and E. B. Bierhaus (2006), The importance of secondary cratering to age constraints on planetary surfaces, *Annu. Rev. Earth Planet. Sci.*, *34*, 535–567.

Michael, G. G., and G. Neukum (2010), Planetary surface dating from crater size-frequency distribution measurements: Partial resurfacing events and statistical age uncertainty, *Earth Planet. Sci. Lett.*, doi:10.1016/j.epsl.2009.12.041.

Moore, J. M., and A. D. Howard (2005), Large alluvial fans on Mars, *J. Geophys. Res.*, *110*, E04005, doi:10.1029/2004JE002352.

Moore, J. M., A. D. Howard, W. E. Dietrich, and P. M. Schenk (2003), Martian layered fluvial deposits: Implications for Noachian climate scenarios, *Geophys. Res. Lett.*, *30*(242292), doi:10.1029/2003GL019002.

Morgan, A. M., A. D. Howard, D. E. Hobley, J. M. Moore, W. E. Dietrich, R. M. E. Williams, D. M. Burr, J. A. Grant, S. A. Wilson, and Y. Matsubara (2014), Sedimentology and climatic environment of alluvial fans in the Martian Saheki crater and a comparison with terrestrial fans in the Atacama Desert, *Icarus*, *229*, 131–156.

Newsom, H. E., et al. (2010), Inverted channel deposits on the floor of Miyamoto Crater, Mars, *Icarus*, *205*, 64–72.

Parker, G. (2008), *Sedimentation Engineering: Processes, Measurements, Modeling, and Practice*, vol. 110, edited by M. H. Garcia, pp. 165–251, American Society of Civil Engineers, Reston, Va.

Parker, G., C. Paola, K. X. Whipple, and D. Mohrig (1998), Alluvial fans formed by channelized fluvial and sheet flow. I: Theory, *J. Hydraul. Eng.*, *124*(10), 985–995.

Parker, T. J., M. C. Malin, F. J. Calef, H. E. Gengl, M. P. Golombek, J. R. Hall, O. Pariser, M. Powell, R. S. Sletten, and the MSL team (2013), Localization and "Contextualization" of Curiosity in Gale Crater, and other landed Mars missions, Lunar and Planetary Sci. Conf. XLIV, Abstract 2534.

Pepin, E., S. Carretier, J. L. Guyot, and F. Escobar (2010), Specific suspended sediment yields of the Andean rivers of Chile and their relationships to climate, slope, and vegetation, *Hydrol. Sci. J.*, *55*(7), 1190–1205, doi:10.1080/02626667.2010.512868.

Stock, J. D. (2012), Waters divided: A history of alluvial fan research and a view of its future, in *Treatise on Geomorphology*, vol. 9, edited by J. Shroder and E. Wohl, pp. xx–xx, Academic Press, San Diego, Calif.

Stock, J. D., K. M. Schmidt, and D. M. Miller (2008), Controls on alluvial fan long profiles, *Geol. Soc. Am. Bull.*, *120*(5–6), 619–640, doi:10.1130/B26208.1.

Sumner, D. Y., et al. (2013), Preliminary geologic map of the Peace Vallis fan integrated with in-situ mosaics from the Curiosity rover, Gale Crater, Mars, Lunar and Planetary Sci. Conf. XLIV, Abstract 1699.

Syvitski, J. P. M., S. D. Peckham, R. Hilberman, and T. Mulder (2003), Predicting the terrestrial flux of sediment to the global ocean: A planetary perspective, *Sediment. Geol.*, *162*(1–2), 5–24.

Thomson, B. J., N. T. Bridges, R. Milliken, A. Baldridge, S. J. Hook, J. K. Crowley, G. M. Marion, C. R. de Souza, A. J. Brown, and C. M. Weitz (2011), Constraints on the origin and evolution of the layered mound in Gale Crater, Mars using Mars Reconnaissance Orbiter data, *Icarus*, *214*(2), 413–432, doi:10.1016/j.icarus.2011.05.002.

Vaniman, D. T., et al. (2014), Mineralogy of a mudstone on Mars, *Science*, *343*, doi:10.1126/science.1243480.

Warner, N. H., S. Gupta, J. R. Kim, J. P. Muller, L. L. Corre, J. Morley, S. Y. Lin, and C. McGonigle (2011), Constraints on the origin and evolution of Iani Chaos, Mars, Mars, *J. Geophys. Res.*, *116*, E06003, doi:10.1029/2010JE003787.

Williams, K. E., O. B. Toon, J. L. Heldmann, C. McKay, and M. T. Mellon (2008), Stability of mid-latitude snowmelts on Mars, *Icarus*, *196*(2), 565–577, doi:10.1016/j.icarus.2008.03.017.

Williams, K. E., O. B. Toon, J. L. Heldmann, and M. T. Mellon (2009a), Ancient melting of mid-latitude snowpacks on Mars as a water source for gullies, *Icarus*, *200*(2), 418–425, doi:10.1016/j.icarus.2008.12.013.

Williams, R. M. E., R. P. Irwin III, and J. R. Zimbelman (2009b), Evaluation of paleohydrologic models for terrestrial inverted channels: Implications for application to Martian sinuous ridges, *Geomorphology*, *107*(3–4), 300–315, doi:10.1016/j.geomorph.2008.12.015.

Williams, R. M. E., A. D. Rogers, M. Chojnacki, J. Boyce, K. D. Seelos, C. Hardgrove, and F. Chuang (2011), Evidence for episodic alluvial fan formation in far western Terra Tyrrhena, Mars, *Icarus*, *211*(1), 222–237, doi:10.1016/j.icarus.2010.10.001.

Williams, R. M. E., R. P. Irwin III, D. M. Burr, T. Harrison, and P. McClelland (2013a), Variability in Martian sinuous ridge form: Case study of Aeolis Serpens in the Aeolis Dorsa, Mars, and insight from the Mirackina paleoriver, South Australia, *Icarus*, *225*, 308–324, doi:10.1016/j.icarus.2013.03.016.

Williams, R. M. E., et al. (2013b), Martian fluvial conglomerates at Gale Crater, *Science*, *340*, 1068–1072, doi:10.1126/science.1237317.

Wilson, L., G. J. Ghatan, J. W. Head III, and K. L. Mitchell (2004), Mars outflow channels: A reappraisal of the estimation of water flow velocities from water depths, regional slopes, and channel floor properties, *J. Geophys. Res.*, *109*, E09003, doi:10.1029/2004JE002281.

Wilson, S. A., J. A. Grant, and A. D. Howard (2012), Distribution of intra-crater alluvial fans and deltaic deposits in the southern highlands of Mars, Lunar and Planetary Sci. Conf. XLIII, Abstract 2462.

Woodsworth, R., F. Forget, E. Millour, J. W. Head, J. B. Madeleine, and B. Charnay (2013), Global modeling of the early Martian climate under a denser CO2 atmosphere: Water cycle and ice evolution, *Icarus*, *222*(1), 1–19, doi:10.1016/j.icarus.2012.09.036.